Genetic analysis of neurons involved in sleep-wake regulation

(睡眠制御に関わる神経細胞の遺伝学的手法を用いた解析)

令和元年度

柏木光昭
所属（筑波大学大学院人間総合科学研究科感性認知脳科学専攻）

Table of contents

Abstract
General introduction
Methods
Results
Chapter1; *Nts*-neurons in the SubLDT are involved in NREM sleep regulation
Chapter2; *Nts*-neurons in the SubLDT send axons to other brainstem areas that also express *Nts*, and chemogenetic activation of putative downstream *Nts*-neurons also promote NREM sleep
Chapter3; Neurotensin peptide is involved in sleep regulation
Discussion
Acknowledgements
References
Figures

Abstract

Mammalian sleep comprises two distinct states, rapid eye movement (REM or paradoxical) sleep and non-REM (NREM) sleep. Classical transection and pharmacological studies suggest that, in addition to the hypothalamus, the brainstem is essential for REM and NREM sleep. The role of the pons in REM sleep has been actively studied, however, those that of in NREM sleep remains less clear. Here, I identified a circuit distributed in the midbrain, pons, and medulla that promotes NREM sleep in mice. I focused on the sublaterodorsal tegmentum (SubLDT), an area implicated in dual regulation of REM and NREM sleep. Chemogenetic activation of the neurons positive for the neuropeptide neurotensin promote NREM sleep. In contrast, functional inactivation of these neurons with tetanus toxin resulted in decrease of NREM sleep, suggesting that these neurons play important role for NREM sleep regulation. Subsequent anterograde tracing and chemogenetic analyses identified putative downstream NREM sleep-promoting neurons in the dorsal deep mesencephalic nucleus (dDpMe), lateral part of the periaqueductal gray (lPAG), and medial vestibular nucleus (MVe), all of which were located in the brainstem and previously unknown population for regulating NREM sleep. Remarkably, all of these putative downstream NREM sleep promoting neurons were also neurotensinergic. Infusion of neurotensin peptide into the fourth ventricle, which faces dorsal surface of the pons and medulla, induced a behavioral quiescent with NREM sleep-like cortical activity. In contrast, mice deficient for neurotensin exhibited increased REM sleep, implicating the involvement of the neuropeptide itself. These findings identify a widely distributed NREM sleep-regulating circuit in the brainstem with a common molecular property.

General introduction

Epidemiologic studies, lesion studies, and circuit genetics studies have demonstrated the involvement of the hypothalamus in sleep regulation. In 1910s, Constantin von Economo, a neurologist in Austria, reported that the neural basis of sleep in human (Von Economo, 1930). According to his study, lesion at the junction of the brainstem and forebrain caused prolonged sleepiness, whereas the lesion in the anterior hypothalamus caused prolonged insomnia. Based on these observations, some researchers proposed that, within the hypothalamus, the anterior part is a sleep promoting center and posterior part is a wake protmoitng center. This finding was further supported by the animal studies showing that lesions in the anterior hypothalamus actually lead to insomnia (Nauta, 1946; Sallanon *et al.*, 1989). Furthermore, a c-fos mapping study, which can estimate the activation of neural activity, showed that neurons in the ventrolateral part of the preoptic hypothalamus were activated during sleep, suggesting that their activity truly contribute to sleep (Sherin *et al.*, 1996). Recently, there was an advance in the development of opto- or chemo-genetics. These tools allow the researchers to manipulate neural activity in a cell type specific manner with high temporal resolution (Adamantidis *et al.*, 2007; Armbruster *et al.*, 2007). By utilizing these methods, many study found and supported that genetic activation of a subpopulation of neurons in the ventrolateral preoptic area rapidly increases sleep (Saito *et al.*, 2013; Zhang *et al.*, 2015; Chung *et al.*, 2017; Kroeger *et al.*, 2018). Furthermore, a recent study revealed that neuroendocrine cells around the hypothalamic supraoptic nucleus also make a large contribution (Jiang-Xie *et al.*, 2019). Together, these studies support a critical role of the hypothalamus in the positive regulation of sleep.

The brainstem is also essential for sleep and wakefulness. In 1940s, ascending reticular activating system was proposed by the electrical stimulation study. Electrical stimulation of the reticular formation in the cat midbrain produces global electroencephalogram desynchronization, indicating these systems play essential roles for controlling wakefulness (Moruzzi and Magoun, 1949). Recently, it was also suggested that the neurons in the lateral part of the parabrachial nucleus, which also locates in the brainstem, is critical for maintaining wakefulness (Fuller *et al.*, 2011). In this study, they found that lesion in the lateral part of the parabrachial nucleus caused an irreversible coma state, indicating that they are crucial for maintaining wakefulness and cortical desynchronization. In addition to these crucial roles for wakefulness, many study suggested that the brainstem is also critical for sleep. Transecting the middle part of the pons results in a long-lasting insomniac state (Batini *et al.*, 1958). Thus, it seems that some neural circuits encompassing this area likely play crucial roles in sleep. Mammalian sleep comprises two distinct states, rapid eye movement (REM or paradoxical) sleep and non-REM (NREM) sleep. After the discovery of REM sleep in 1953 (Aserinsky and Kleitman, 1953), the role of the pons in REM sleep has been actively studied. Neurons that fire maximally during REM sleep were identified in the dorsolateral pontine

tegmental area, especially around the peri-locus coeruleus alpha in cats (Sakai, 1988). Subsequently, the sublaterodorsal tegmental nucleus (SubLDT) in rodents was identified as a homologous structure to the cat peri-LC alpha (Boucetta *et al.*, 2014; Sakai, 2015). Application of carbachol or bicuculline to these areas can induce REM sleep with a short latency (Vanni-Mercier *et al.*, 1989; Boissard *et al.*, 2002), whereas lesions result in reduced REM sleep (Sastre, Sakai and Jouvet, 1981; Lu *et al.*, 2006). c-fos mapping studies in rodents were also conducted to see the relationship between neural activity and REM sleep (Sapin *et al.*, 2009; Clément *et al.*, 2011). These study suggested that glutamatergic neurons are activated after deprivation-induced REM sleep rebound. The cell-type specific studies, utilizing Cre-loxP gene recombination or RNAi to specifically inactivate glutamatergic transmission, support their contribution to REM sleep (Krenzer *et al.*, 2011; Valencia Garcia *et al.*, 2016).

By contrast, the precise pontine circuitry that promotes NREM sleep is less clear. GABAergic neurons located in the medullar region, termed the parafacial zone (PZ), contribute to NREM sleep. These neurons project to the pontine parabrachial nucleus, and their functional inhibition results in increased wakefulness (Anaclet *et al.*, 2012, 2014). Single unit recording study showed that there are NREM sleep active inhibitory neurons in the ventrolateral periaqueductal gray (vlPAG)/ dorsal deep mesencephalic nucleus (dDpMe) (Crochet, Onoe and Sakai, 2006; Sakai, 2018). Optogenetic or chemogenetic activation of these neurons promote NREM sleep and at least some of their effects are relying on its projections to the dorsal pons (Hayashi *et al.*, 2015; Weber *et al.*, 2018). The severe insomniac phenotype following pons transection, however, implies that other brainstem neurons also promote NREM sleep.

Here, I focused on the SubLDT, which, as described above, is critical for REM sleep. In addition to crucial roles in REM sleep generation, activation of a subpopulation of glutamatergic neurons in the SubLDT has the opposite effect: increasing NREM sleep and reducing REM sleep (Hayashi *et al.*, 2015). Electrophysiologic studies revealed neurons in this area that actively fire during NREM sleep, further supporting the involvement of the SubLDT in the dual regulation of both REM and NREM sleep (Sakai, 2015). Thus, this area represents a complex structure in which neurons of diverse subtypes and functions are intermingled, and genetic approaches are crucial to further analyze the involvement of each subtype in controlling sleep (Weber and Dan, 2016).

In the present study, I attempted to isolate molecular markers for neurons in the SubLDT that critically regulate sleep. The identification of a molecular marker for neurons promoting NREM sleep allowed to further analyze the downstream neurons and molecular mechanisms.

Materials and methods

Animals.

All animal experiments were approved by the institutional animal care and use committee of the

University of Tsukuba. All animals were maintained according to the institutional guidelines of the Laboratory of Animal Resource Center, University of Tsukuba. For *Nts-Cre* mice, the pgk-neo cassette (*frt-pgk-neo*) was removed by crossing with the *Flippase* deleter strain. For chemogenetic experiments, male and female mice at least 6 weeks old were used. For tetanus-toxin (TeTx) expression experiments, male littermate mice at least 8 weeks old were randomly assigned to the experimental or control group. Mouse genotyping was performed using following primer pairs: *frt-pgk-neo* 5'- TCGGCCATTGAACAAGATGG -3' & 5'- TCGTCAAGAAGGCGATAGAAGG -3'; *Atoh1-CreER*^{T2} , 5'- GACGATGCAACGAGTGATGA-3' & 5'- AGCATTGCTGTCACTTGGTC-3'; *Chat-Cre*, 5'-GCAAAGAGACCTCATCTGTGGA-3' & 5'-CAGGGTTAGTAGGGGCTGAC-3' & 5'-CAAAAGCGCTCTGAAGTTCCT-3', *Nts-Cre* 5'-ATAGGCTGCTGAACCAGGAA-3' & 5'-CAATCACAATCACAGGTCAAGAA-3' & 5'-CCAAAAGACGGCAATATGGT-3', Ai9; 5'-AAGGGAGCTGCAGTGGAGTA-3' & 5'-CCGAAAATCTGTGGGAAGTC-3' & 5'-GGCATTAAAGCAGCGTATCC-3' & 5'-CTGTTCCTGTACGGCATGG-3', *Rosa26-CAG-loxP-STOP-loxP-Rpl10a-GFP*; 5'-AAGGGAGCTGCAGTGGAGTA-3' & 5'-CCGAAAATCTGTGGGAAGTC-3' & 5'-GGCATTAAAGCAGCGTATCC-3' & 5'-AAGATCCGCCACAACATCG-3', TTCTCGTTGGGGTCTTTGCT -3', *Nts*-knockout ; 5'-GCACCGAGAGAGAGCTAGCT-3' & 5'-GCAGACTGCGAGAGAAATCCC-3' & 5'-GCGTTTCACCCTGCCATAA-3'. All mice were provided free access to food and water, with a 12-h light-dark cycle. All mice used in this study were group-housed (2-5 mice/cage) before surgery and single-housed after surgery.

Virus preparation.

To generate plasmid pAAV-*hSyn-DIO-GFP-T2A-TeTx*, the *hM3Dq-mCherry* segment of pAAV-*hSyn-DIO-hM3Dq-mCherry* was replaced with a polymerase chain reaction (PCR) fragment containing *GFP-T2A-TeTx*. These plasmids were packaged in serotype8 as previously described (Yasuda *et al.*, 2017). Briefly, HEK293T cells were transfected with pAAV-*hSyn-DIO-GFP-T2A-TeTx*, pHelper, and pSerotype8 plasmids. At 72 h after transfection, the virus-containing media were ultracentrifuged at 23,000 rpm for 2 h with 20% sucrose/phosphate buffer saline (PBS) (w/v) cushion. After pouring out the supernatant, viruses in the pellets were resuspended in cold PBS and stored at -80°C until use. Viral titer of AAV-*hSyn-DIO-GFP-T2A-TeTx* (serotype8, titer: $3.8x10^{13}$ vg/ml) was determined by qPCR using a primer pair for GFP (forward: 5'-AAGATCCGCCACAACATCG -3', reverse: 5'- AAGATCCGCCACAACATCG -3'). AAV-*hSyn-DIO-hM3Dq-mCherry* (serotype2, titer: $5.1x10^{12}$ vg/ml), AAV-*hSyn-DIO-mCherry* (serotype8, titer: $3.8x10^{12}$ vg/ml and serotype2, titer: $3.1x10^{12}$ vg/ml), AAV-*hSyn-flex-tdTomato-T2A-synaptophysin-GFP* (serotype1, titer: $1.1x10^{12}$ vg/ml), and AAV-*hSyn-flex-GCaMP6s* (serotype5, titer: $6.7x10^{12}$ vg/ml) were purchased from UNC vector core, Salk vector core, or University of

Pennsylvania Vector Core, respectively. For AAV-*hSyn-DIO-hM3Dq-mCherry* and AAV-*hSyn-DIO-GFP-T2A-TeTx*, we confirmed that there was no Cre independent expression of the transgene by verifying mCherry and GFP expression in the sections of WT mice injected with each virus.

Surgery

Mice were anesthetized with isoflurane and placed in a stereotaxic apparatus (Leica Angle Two) and the height of bregma and lambda was adjusted to be within a difference of 0.1 mm. AAV vector for SubLDT (0.05-0.1 µl), dDpMe (0.1 µl), lPAG (0.1 µl), and MVe (0.2-0.3 µl) was microinjected at a speed of 0.01-0.03 µl/min using a glass capillary and a syringe pump (KD Scientific 210). Target locations were as follows: SubLDT: (medio-lateral (ML), ±0.7 mm; antero-posterior (AP), -5.2 mm; dorso-ventral (DV), -4.1 mm) dDpMe: (ML, ±0.5 mm; AP, -4.5 mm; DV, -3.5 mm), lPAG: (ML, ±0.5 or +0.5 mm; AP, -4.8 mm; DV, -2.5 mm), MVe: (ML, ±0.8 mm; AP, -5.9 mm; DV, -4.5 mm). After AAV microinjection, EEG (electroencephalogram) and EMG (electromyogram) electrodes were implanted. Electrodes (stainless steel recording screws) for EEG were implanted epidurally over the parietal area (1 mm anterior to lambda, 1 mm lateral to midline) referenced to the cerebellum area. EMG electrodes were bilaterally implanted into the neck muscle. For ICV injection, cannula implantation was performed as previously described (Iwasaki *et al.*, 2018). A 27G stainless steel tube (10 mm) was inserted into the fourth ventricle (target: ML, 0 mm; AP, -6.0 mm; DV, -4.0 mm) and EEG/EMG electrodes were implanted as described above.

EEG/EMG recording and analysis

For chemogenetic experiments, mice were allowed to recover for at least 2 weeks after surgery. The mice were then moved to a sleep recording chamber and connected to an amplifier for EEG/EMG recording. For acclimatization, the mice were administered vehicle (saline) by intraperitoneal injection at ZT 5 for 5 days or at ZT 17 for 2 days. EEG/EMG signals were recorded for at least 6 h beginning 1 min after the drug administration. In each mouse, EEG/EMG was recorded at least twice for vehicle and CNO, respectively, and the mean value for each condition was calculated, except for Figures 3A-3C, where a single set was applied for analysis. For tetanus toxin experiments, we recorded EEG/EMG for 24 h at 4 weeks after surgery. For ICV administration, mice were allowed to recover at least 1 week after surgery. For acclimatization, 1 µl of vehicle (saline) was infused daily at ZT 5 for at least 3 days. After that, on the first day, we recorded EEG/EMG for 6 h after saline infusion. On the next day, we recorded EEG/EMG with infusion of neurotensin peptide solution. For administration, we used a 27G stainless steel tube connected to a Hamilton syringe with plastic tubing. For comparison of *Nts*-knockout mice and WT littermates, mice were acclimatized to the sleep chamber for 1 week and EEG/EMG was recorded for at least 24 h. EEG/EMG analyses were conducted by a researcher blind to the mouse genotype. After sleep recording, genotypes were

reconfirmed by PCR.

EEG/EMG signals were filtered (band pass 0.5-64Hz) and collected and digitized at a sampling rate of 128 Hz via VitalRecorder (Kissei comtec). EEG signals were subjected to fast fourier transform and further analysis using SleepSign (Kissei Comtec). The vigilance state in each epoch was manually classified as REM sleep, NREM sleep, or wake based on absolute delta (0.5-4 Hz) power, theta (6-10 Hz) power to delta power ratio, and the integral of EMG signals. We applied 4-s epochs throughout the study except for studies related to the SubLDT *Nts*-neurons, where 10-s epochs were applied. If a single epoch contained multiple states, the state with the highest occupancy was assigned.

Drug preparation

Clozapine-N-Oxide (Sigma; C0832) was prepared at 5 mg/ml in milliQ and diluted with saline. For sleep recording experiments, CNO was administered at a dose of 1.5 mg/kg body weight. For c-fos staining, CNO was administered at a dose of 4.5 mg/kg body weight, and mice were perfused 2 h after administration. For ICV administration, neurotensin synthetic peptide (PEPTIDE INSTITUTE, INC.: 4029-v) solution was prepared at a concentration of 20 ng/µl with saline before the experiment.

Preparation and administration of tamoxifen

Tamoxifen (7.5 mg/ml) was prepared by dissolving 60 mg of tamoxifen (Sigma;T5648) in 4 ml of ethanol, and then adding 8 ml of sunflower seed oil (Sigma; S5007) and mixing thoroughly by vortex and sonication in a ultrasonic cleaner. Finally, ethanol was removed with a centrifugal evaporator. To label *Atoh1*-neurons with EYFP, female *Atoh1-CreER*^{T2} mice (Hayashi *et al.*, 2015) were crossed with male *Rosa26-CAG-loxP-STOP-loxP-EYFP* reporter mice (Madisen *et al.*, 2010). Tamoxifen (1.05 mg) was administered orally 11 days after detection of vaginal plugs, before noon. The progeny carrying double transgenes were used for histologic analyses.

Histology

Deeply anesthetized mice were killed by injecting lethal doses of anesthetics and underwent transcardial perfusion with 0.1 M PBS followed by 4% paraformaldehyde (w/v) in 0.1 M PBS. After extraction, the brains were postfixed in the same fixative at least overnight and subsequently equilibrated in 30% sucrose (w/v) in PBS. The brains were sectioned at 30-50 µm using a sliding microtome (Yamato Kohki).

Immunohistochemistry (IHC)

The sections were washed 3x 5 min in TBST (1xTBS, Tris-buffered saline (pH 7.5) + 0.1% Tween20), 3 min 0.3% H_2O_2/1xTBS, and washed 3x 5 min in TBST. Non-specific binding was blocked by

incubation in TBS blocking buffer (1xTBS + 0.5% Blocking Reagent (Perkin Elmer; FP1020)) for 30 min. The sections were then incubated overnight with a primary antibody for mCherry (1/500: rabbit anti-red fluorescent protein (RFP) (MBL, PM006), 1/2000: goat anti-RFP (SICGEN; AB8181-200)), GFP (1/500: rat anti-GFP (Nacalai tesque; GF090R), or c-fos (1/2000: rabbit anti-c-fos (Calbiochem; PC38)) at 4°C or for Chat (1/100: goat anti-Choline acetyltransferase (Chat) Millipore; AB144P) or c-fos (1/2000: rabbit anti-c-fos (Millipore ;ABE457) at room temperature. After 3x 5 min wash in TBST, the sections were incubated with a secondary antibody (1/500: donkey anti-rabbit-HRP (Abcam; ab7083), 1/500: donkey anti-rat -HRP (Abcam; ab102182), or CF-conjugated antibodies (1/500: BIOTIUM)) and 1 μg/ml DAPI for 2 h. After 4x 5 min wash in TBST, the sections were incubated with tyramide reagent (Perkin Elmer) for 30 min. Finally, after washing 4x 5 min in TBST, the sections were mounted on a slide glass using mounting medium (PermaFluor; TA-006-FM). Images were captured with a laser confocal microscope (Carl Zeiss; LSM700, LSM800) or NanoZoomer (Hamamatsu).

In situ hybridization (ISH)/IHC double staining

Antisense digoxigenin (DIG)-labeled RNA probe were used in this study. Template DNA sequences of *Vesicular glutamate transporter2 (Vglut2)* and *Vesicular gaba transporter (Vgat)* were designed as shown in the Allen Brain Atlas (http://mouse.brain-map.org/) (*Vglut2*; RP_050921_01_E03, *Vgat*; RP_07124_02_A05). Plasmids containing a template cDNA for *Nts* were obtained from Riken FANTOM. We used a region amplified with PCR primer; 5'-tgacagttcactcactttga-3' and 5'-cctgatggcttgttgacttt-3'.

Sections were incubated in methanol for 15 min and washed 3x 5 min with PBST (1xPBS + 0.1% Tween20). The sections were then incubated in 10 μg/ml proteinase K (Roche; 03115887001) at 37°C for 10 min and washed 2x 5 min with PBST. The sections were then fixed in 4% paraformaldehyde/PBS for 20 min and washed 3x 5 min with PBST. DIG-labeled RNA probes (1 μg/ml) in 50% formamide/5x standard saline citrate (SSC)/0.1% Tween 20 were added to the sections and incubated at 60°C overnight. Subsequently, sections were washed with 50% formamide/2x SSC/0.1% Tween 20 at 60°C for 60 min, 2x SSC/0.1% Tween 20 at 60°C for 15 min, and 0.2x SSC/0.1% Tween 20 at 60°C for 60 min. The sections were then washed 3x 5 min with TBST, and incubated overnight with anti-alkaline phosphatase (AP) labeled DIG antibody (1/1,000 anti-DIG-AP (Roche; 11093274910)) at 4°C. After washing 3x 5 min in TBST and 3x 5 min in 0.1M Tris-HCl (pH8.2)/0.1% Tween 20, sections were incubated in the HNPP/Fast Red solution (Roche; 11758888001) for 0.5-2 h and washed again in TBST 3x 5 min. Subsequently, IHC for YFP or mCherry was performed. Briefly, sections were incubated overnight with primary antibodies for YFP (1/100: rabbit anti-denatured GFP (Santa Cruz Biotechnology; SC8344), RFP (1/100: rabbit anti-RFP [MBL; PM006], 1/250 goat anti-RFP [SICGEN; AB8181-200]) at 4°C, followed by secondary

antibody staining using CF-conjugated antibodies (1/500: BIOTIUM). For detection of synaptophysin-GFP, GFP signals were amplified with tyramide signal amplification (TSA) as described for IHC. In some cases, a Fast Red reaction was performed again after IHC due to its signal diffusion. We confirmed that the ISH procedure eliminates the native fluorescence. Images were captured with a laser confocal microscope (Carl Zeiss; LSM700, LSM800).

Quantification and Statistics

The statistical details of the experiments are provided in the figure legends. Sample size was determined based on previous relevant studies. Graph represents mean±SEM. Data were analyzed with Prism (Graph Pad) or SPSS (IBM). A p-value of less than 0.05 was considered statistically significant.

Results

Chapter1: *Nts*-neurons in the SubLDT are involved in NREM sleep regulation

A subset of glutamatergic neurons in the SubLDT developmentally originate from the cerebellar rhombic lip and transiently express *Atoh1* (*Mouse atonal homolog 1* or *Math1*) during embryonic days 10-12 in mice (Machold and Fishell, 2005; Wang, Rose and Zoghbi, 2005). Subsequent chemogenetic analyses demonstrated that these *Atoh1* lineage neurons (*Atoh1*-neurons) participate in promoting NREM sleep (Hayashi *et al.*, 2015). To explore the molecular identity of *Atoh1*-neurons in adults, transcriptomics analyses were previously conducted by my superviser, Dr. Yu Hayashi. Tissues from the SubLDT and adjacent control areas, either dorsomedial (LDT) or ventral (pontine reticular nucleus) to the SubLDT, were collected and the total RNA was subjected to microarray analyses. The most statistically outstanding candidate gene was *Nts*, which encodes the 13-amino acid neuropeptide neurotensin. To begin address the functions of *Nts* positive neurons for sleep-wake regulation, I attempted to examine whether *Atoh1*-neurons overlap with *Nts*.

Results and Discussion

Identification of *Nts* as a candidate marker gene for NREM sleep-promoting neurons in the SubLDT

First, I performed fluorescent *in situ* hybridization (ISH) to confirm *Nts* is actually expressed in the SubLDT. As a result, *Nts* is strongly expressed in a subset of cells in the SubLDT (Figure 1A). To see the overlap between *Atoh1*-neurons and *Nts*-expressing cells, mice double transgenic for *Atoh1-CreER*^{T2} (Hayashi *et al.*, 2015) and *Rosa26-CAG-loxP-STOP-loxP-EYFP* (Ai3) (Madisen *et al.*, 2010) were administered tamoxifen at embryonic day 11, allowing *Atoh1*-neurons to be labeled by enhanced yellow fluorescent protein (EYFP), and subjected to double staining for *Nts* (ISH) and YFP (IHC). These mice were prepared by Ms. Mika Kanuka. The *Nts*$^{+}$ cells comprised 95% of

EYFP$^+$ cells, and the EYFP$^+$ cells comprised 45% of *Nts*$^+$ cells (Figures 1B and 1C), suggesting a large overlap between the two groups of cells. The presence of some EYFP$^-$ *Nts*$^+$ cells might be due in part to the sparse labeling nature of the CreER^{T2} system.

Nts-neurons in the SubLDT were mainly glutamatergic, while some were GABAergic, and none were cholinergic.

I utilized Cre-loxP gene recombination technique to selectively label *Nts*-neurons in the SubLDT. *Nts-Cre* mice (Leinninger *et al.*, 2011) were crossed with GFP reporter mice (*Rosa26-CAG-loxP-STOP-loxP-Rpl10a-GFP*) or locally injected adeno-associated virus carrying Cre dependent GCaMP6s. These mice were subjected to the histological analysis. *Nts*-neurons in the SubLDT overlap with endogenous *Nts* mRNA. Furthermore, they were mainly glutamatergic, while some were GABAergic, and none were cholinergic, based on the co-expression of *vesicular glutamate transporter 2 (Vglut2)*, *vesicular gaba transporter (Vgat)*, or choline acetyltransferase (Chat), respectively (Figures 1D-1G).

Chemogenetic activation of _Nts_-neurons in the SubLDT promote NREM sleep

To evaluate the effect of activation of *Nts*-neurons in SubLDT on sleep-wake states, I first took a chemogenetic approach – DREADD (Designer Receptors Exclusively Activated by Designer Drug) (Armbruster *et al.*, 2007). AAV encoding Cre-inducible hM3Dq receptor (AAV-*hSyn-DIO-hM3Dq-mCherry*) was bilaterally injected into the SubLDT of *Nts-Cre* mice (Figures 2A-2C). hM3Dq is a genetically engineered Gq-coupled receptor that causes neural excitation upon binding of its selective synthetic ligand clozapine-N-oxide (CNO). CNO administration induced the expression of c-fos (Figure 2D), which is an *in vivo* marker of neuronal excitation. Next, I recorded the electroencephalogram (EEG)/ electromyogram (EMG) and compared vigilance states following vehicle (saline) or CNO (1.5 mg/kg) administration, respectively. When *Nts*-neurons were activated at Zeitgeber Time (ZT) 5, NREM sleep was increased at the expense of both wakefulness and REM sleep, with an especially strong effect on REM sleep (Figures 2E-2G). Further analysis revealed that mean wake episode duration and REM episode number were reduced (Figures 2H-2J). Chemogenetic activation of *Nts*-neurons in the dark phase (ZT17) also increased NREM sleep and decreased wakefulness, while the effect on REM sleep was not significant perhaps due to the low basal amount (Figure 2K).

Notably, when I analyzed sleep for a longer period, i.e. 24 hours, after chemogenetic activation of SubLDT *Nts*-neurons at ZT5, the initial increase in NREM sleep amount was followed by a subsequent decrease (Figures 3A-3C). Thus, the induced NREM sleep might be under homeostatic regulation, similar to spontaneous NREM sleep. When CNO was administered to *Nts-Cre* mice injected with control AAV encoding mCherry (AAV-*hSyn-DIO-mCherry*), there was no

effect on the amount of each state (Figure 3D), indicating that the observed effect is not due to CNO or its derivatives. The inhibitory effect on wakefulness contrasts with the effect of activation of *Atoh1*-neurons, which decreased REM sleep but not wakefulness. The difference between the effect on wakefulness might be due to the larger number of *Nts*-neurons compared with *Atoh1*-neurons.

Functional inactivation of *Nts*-neurons in the SubLDT inhibit NREM sleep

Next, I functionally inhibited *Nts*-neurons to examine whether they are crucial for maintaining normal sleep-wake structures. I disrupted synaptic transmission by expressing the tetanus toxin light chain (TeTx) (Nakashiba *et al.*, 2008), an endopeptidase specific for VAMP2, in a cell type-specific manner. AAV encoding Cre-inducible TeTx (AAV-*hSyn-DIO-GFP-2A-TeTx*) was injected into the SubLDT of *Nts-Cre* mice (Figures 4A-4C). Compared with control mice injected with AAV-*hSyn-DIO-mCherry*, the amount of NREM sleep was decreased (Figure 4D). NREM sleep reduction occurred mainly in the dark phase, with a concomitant increase in wakefulness. By contrast, the increase in the REM sleep occurred only during the light phase, perhaps because during the dark phase, the effect of wakefulness induction was more dominant. For REM sleep, the mean episode duration was shortened whereas the episode number was increased (Figures 4E-4H), an effect similar to that produced by lesions of this area (Lu et al., 2006), providing further support that these neurons are an important component of the REM sleep/NREM sleep switch. These findings indicate that *Nts*-neurons in the SubLDT are important for maintaining natural sleep-wake cycles.

Chapter2:

Nts-neurons in the SubLDT send axons to other brainstem areas that also express _Nts_, and chemogenetic activation of putative downstream _Nts_-neurons also promote NREM sleep

Introduction

In the Chapter1, I identified that *Nts*-neurons in the SubLDT are involved in NREM sleep regulation. I next attempted to examine downstream mechanism. To see the projection targets of *Nts*-neurons in the SubLDT, I injected viral vector encoding a synaptophysin-GFP, which localizes pre-synapses. As a result, I found that *Nts*-neurons in the SubLDT send axons to other brainstem nuclei, all of which also express *Nts*. Furthermore, chemogenetic activation of these putative downstream *Nts*-neurons also induced NREM sleep, suggesting that common molecular property of NREM sleep promoting neurons in the brainstem.

Results and Discussion

Nts-neurons in the SubLDT send axons to other brainstem areas that also express _Nts_

To identify possible downstream targets, I visualized presynaptic structures of these neurons by injecting AAV encoding synaptophysin fused to GFP (AAV-*hSyn-flex-tdTomato-2A-synaptophysin-GFP*) into the SubLDT of *Nts-Cre* mice (Figures 5A and 5B). GFP signals were detected in the dorsal deep mesencephalic nucleus (dDpMe), lateral part of the periaqueductal gray (lPAG), and medial vestibular nucleus (MVe), all of which are located in the brainstem (Figures 5C and 5D). Interestingly, a subset of cells in these brain areas also expressed *Nts*, and their soma were in close proximity to the labeled presynaptic structures, suggesting that SubLDT *Nts*-neurons project to *Nts*-neurons in these brainstem areas (Figures 5D and 5E). This observation lead me to further investigate the roles of these downstream *Nts*-neurons in sleep regulation.

Activation of putative downstream *Nts*-neurons also increased NREM sleep

I again used chemogenetics to examine the effects of activating *Nts*-neurons in the areas described above on sleep (Figures 6A-6C, 6F-6H, 6K-6M). Upon *hM3Dq-mCherry* expression, CNO administration reliably induced c-fos expression in each brain area (Figures 7A, 7E, and 7I). Activation of *Nts*-neurons in the light phase in either the lPAG, dDpMe, or MVe increased NREM sleep at the expense of both wakefulness and REM sleep (Figures 6D-6E, 6I-6J, 6N-6O, and 8A-8D, 8F-8I, and 8K-8N). Activation in the dark phase also increased NREM sleep (dDpMe and MVe) and decreased the ratio of REM sleep to total sleep (lPAG, dDpMe, and MVe; Figures 8E, 8J, and 8O). Several studies have suggested (Crochet, Onoe and Sakai, 2006; Lu *et al.*, 2006; Sapin *et al.*, 2009) or demonstrated (Hayashi *et al.*, 2015; Weber *et al.*, 2015, 2018) the existence of inhibitory neurons that promote NREM sleep in the dDpMe or adjacent vlPAG, and excitatory neurons in these same regions that induce wakefulness from sleep (Weber *et al.*, 2018). Unexpectedly, *Nts*-neurons in this area were mainly glutamatergic, but not GABAergic, based on the co-expression of *vesicular glutamate transporter 2 (Vglut2)* or *vesicular gaba transporter (Vgat)* (Figures 7B-7D). Thus, my results suggest that, in addition to inhibitory neurons, a subset of glutamatergic neurons in the dDpMe that co-express *Nts* also promote NREM sleep. Similarly, while lesion and tracing studies suggest that there are inhibitory neurons in the lPAG that inhibit REM sleep (Boissard *et al.*, 2003; Lu *et al.*, 2006), *Nts*-neurons in the lPAG are also mainly glutamatergic (Figures 7F-7H). Thus, *Nts*-neurons in the lPAG are also a previously unknown population of NREM sleep-promoting neurons with a glutamatergic nature. By contrast, *Nts*-neurons in the MVe were mainly GABAergic (Figures 7J-7L). Some of these neurons might overlap with previously reported NREM sleep-promoting GABAergic neurons in the PZ (Anaclet *et al.*, 2012, 2014), although the area I targeted was located more dorsal than the areas targeted in these previous reports.

***Nts*-neurons in the lPAG and MVe were activated by sleep deprivation**

To examine the activity pattern of *Nts*-neurons in SubLDT, dDpMe, lPAG, and MVe across

spontaneous sleep-wake cycles, I compared c-fos expression, which is a marker for neural activation, in the *Nts*-neurons between several conditions (Figures 9A-9C). In the lPAG, c-fos expression in *Nts*-neurons was highest after sleep deprivation, suggesting that these neurons are activated by sleep pressure. A similar trend was also observed in the MVe. By contrast, I did not detect any significant differences in c-fos expression among the conditions in case of *Nts*-neurons in SubLDT and dDpMe. Single unit recording studies in mice have shown that, in these 2 areas, the activity pattern of each neuron across sleep-wake is highly diverse (Sakai, 2015, 2018). Therefore, even within the *Nts*-neurons, there might be some heterogeneity, although I cannot exclude the possibility that these neurons do not show any sleep related activity.

Chapter3:
Neurotensin peptide is involved in sleep regulation

Introduction

In the Chapter1 and Chapter2, I identified multiple populations of NREM sleep-promoting neurons that are widely distributed in the brainstem. Remarkably, all these neurons expressed *Nts*. Thus, I next examined whether the neurotensin peptide itself has a role for sleep-wake regulation. To do so, I infused the peptide into the fourth ventricle and examined the effect on sleep-wake state. In addition, I also analyzed the sleep in *Nts*-knock out (KO) mice.

Results and Discussion

Administration of neurotensin peptide rapidly induced NREM sleep-like states

I infused neurotensin into the fourth ventricle, which faces the dorsal surface of the pons and medulla, at ZT5 and measured EEG/EMG (Figure 10A). As a result, a behaviorally quiescent state with cortical slow wave activity and EMG amplitude lower than that in naturally occurring NREM sleep was rapidly induced at the expense of both awake and REM sleep (Figures 10B-10G). A similar effect was observed when neurotensin was administered in the dark phase (ZT17) (Figure 10H). These results imply that neurotensin peptide itself contributes to the regulation of NREM sleep.

Nts-KO mouse showed increased REM sleep

I next measured EEG/EMG and analyzed sleep in *Nts*-deficient mice (Dobner *et al.*, 2001). These mice exhibited an increased amount of REM sleep and an increased ratio of REM sleep to total sleep, compared with their wildtype littermates (Figures 11A-11E). Altogether, these results suggest that neurotensin itself participates in sleep regulation by promoting NREM sleep-like activity and reducing REM sleep-like activity.

General discussion

I found that *Nts* is selectively expressed in a subset of neurons in the SubLDT and that these neurons promote NREM sleep. Projection target analyses of these neurons and subsequent cell type-selective analyses led to further identification of NREM sleep-promoting neurons in other brainstem areas, namely glutamatergic neurons in the dDpMe and lPAG, and GABAergic neurons in the MVe, none of which were previously identified to be involved in sleep regulation. Remarkably, these candidate downstream neurons were also Nts^{+}, revealing a common molecular feature among these brainstem neurons. In the future, it is important to address whether the pathways from SubLDT to these putative downstream neurons are truly functional and important for NREM sleep control. In addition, functional intervention of these neurons had different outcomes depending on the timing of the day, suggesting that these neurons receive a circadian influence of sleep control, which is another important issue to be addressed in the future.

In addition to the brainstem, *Nts* is widely expressed in many brain areas, including the hypothalamus, subthalamic nucleus, striatum, amygdala, and thalamus (Schroeder *et al.*, 2019). Some *Nts*-neurons in these areas also participate in sleep regulation. *Nts*-neurons in the posterior thalamus and central amygdala also promote NREM sleep (Ma *et al.*, 2019), whereas those in the lateral hypothalamus are suggested (Furutani *et al.*, 2013) or demonstrated (Naganuma *et al.*, 2019) to promote wakefulness. Thus, the roles of *Nts*-neurons in sleep regulation appear highly diverse. Importantly, the release of the neurotensin neuropeptide itself is crucial for the function of NREM sleep-promoting neurons in the posterior thalamus and central amygdala (Ma *et al.*, 2019). Similarly, for the NREM sleep-promoting neurons in the brainstem that were identified in this study, neurotensin might support their functions by promoting NREM sleep-like cortical activity and suppressing wake or REM sleep, based on the results of experiments in which neurotensin was infused into the fourth ventricle and those using *Nts*-deficient mice. These my results must be cautiously interpreted, however, as neurotensin has diverse and complicated roles in sleep regulation. For example, neurotensin infused into the third ventricle increases theta oscillation and inhibits sleep (Castel *et al.*, 1989), whereas infusion into the basal forebrain increases both theta and gamma oscillation and increases wakefulness and REM sleep (Cape *et al.*, 2000). The phenotype of *Nts*-deficient mice in the present study likely reflects a summed effect of neurotensin functions in various brain areas. Future studies using conditional knockout mice or other brain region/cell type-selective approaches may further elucidate how neurotensin produced in the brainstem contributes to sleep regulation. Neurotensin signaling also has important roles in pain (Clineschmidt and McGuffin, 1977), blood pressure (Rioux *et al.*, 1981), and metabolism (Leinninger *et al.*, 2011; Li *et al.*, 2016). In the future, it is important to address whether *Nts*-neurons play a role in the coordination among sleep and these other phenomena.

GABAergic neurons in the vlPAG/dDpMe and PZ promote NREM sleep by reducing

both wakefulness and REM sleep. These neurons project to the lateral parabrachial nucleus (Anaclet *et al.*, 2012, 2014) and (in the case of the vlPAG/dDpMe) to the SubLDT (Hayashi *et al.*, 2015; Weber *et al.*, 2018). This appears reasonable, as these downstream areas contain neurons that promote wakefulness or REM sleep, respectively. The GABAergic neurons in the MVe identified in the present study might also project to similar areas. Rhythmic stimulation of the vestibular system promotes sleep in mice (Kompotis *et al.*, 2019). Further studies to address whether MVe GABAergic neurons are involved in this vestibular input-dependent regulation of sleep will provide interesting information. How glutamatergic neurons in the dDpMe and lPAG promote NREM sleep also remains a mystery. Considering that these neurons are excitatory, they likely project to other neurons that also promote NREM sleep within the same brain area or to other areas.

Technical considerations

It should be also noted that I need carefully interpret the data reported from this study. In this study, I used EEG and EMG to define the vigilance state, although this is a common method in this field. For example, monotreme Echidna (*Tachyglossus aculeatus*) have only NREM sleep like state if the states are defined by following criteria of EEG based classification. Importantly, Echidna's EEG-based NREM like state can be clearly classified into two distinct stage both of which seems to be corresponding to mammalian NREM and REM sleep when the signals were taken from brainstem (Siegel *et al.*, 1996). Similarly, activation of *Nts*-neurons in this study might have evoked another sleep stage that compensate the loss of EEG defined REM sleep, which only becomes visible when the signals are taken from subcortical area, brainstem, autonomic nerve system, and so on.

Conclusion

I identified widely distributed neurons in the brainstem that promote NREM sleep. This study provides insight into how the brainstem is involved in regulating sleep. Moreover, I revealed that the identified neurons were all positive for *Nts*. The brainstem is one of the most highly conserved brain structures among vertebrate animals. In the future, in addition to studies of the mutual connections with other known sleep regulating circuits, it would be interesting to address whether homologous *Nts*-neurons exist in vertebrate animals that do not exhibit REM and NREM sleep, which might provide insight into the evolution of the complex mammalian sleep architecture.

Acknowledgements

I thank for Dr. Yu Hayashi for supervising the study, design and support of experiments, and revising the manuscript, Dr. Masashi Yanagisawa for all supports to this study, Ms. Mika Kanuka Ms. Chika Tatsuzawa, Ms. Miho Morita, and Ms. Kaeko Tanaka for assistance and discussion of experiments.

References

Adamantidis, A. R. *et al.* (2007) 'Neural substrates of awakening probed with optogenetic control of hypocretin neurons.', *Nature*, 450(7168), pp. 420–4. doi: 10.1038/nature06310.

Anaclet, C. *et al.* (2012) 'Identification and Characterization of a Sleep-Active Cell Group in the Rostral Medullary Brainstem', *Journal of Neuroscience*, 32(50), pp. 17970–17976.

Anaclet, C. *et al.* (2014) 'The GABAergic parafacial zone is a medullary slow wave sleep-promoting center', *Nature Neuroscience*, 17(9), pp. 1217–1224.

Armbruster, B. N. *et al.* (2007) 'Evolving the lock to fit the key to create a family of G protein-coupled receptors potently activated by an inert ligand', *Proceedings of the National Academy of Sciences*, 104(12), pp. 5163–5168.

Aserinsky, E. and Kleitman, N. (1953) 'Regularly Occurring Periods of Eye Motility, and Concomitant Phenomena, during Sleep', *Science (New York, N.Y.)*, 118(3062), pp. 273–274. doi: 10.1176/appi.neuropsych.15.4.454.

Batini, C. *et al.* (1958) 'Presistent patterns of wakefulness in the pretrigeminal midpontine preparation.', *Science*, 128(3314), pp. 30–32.

Boissard, R. *et al.* (2002) 'The rat ponto-medullary network responsible for paradoxical sleep onset and maintenance: A combined microinjection and functional neuroanatomical study', *European Journal of Neuroscience*, 16(10), pp. 1959–1973.

Boissard, R. *et al.* (2003) 'Localization of the GABAergic and non-GABAergic neurons projecting to the sublaterodorsal nucleus and potentially gating paradoxical sleep onset', *European Journal of Neuroscience*, 18(6), pp. 1627–1639.

Boucetta, S. *et al.* (2014) 'Discharge Profiles across the Sleep-Waking Cycle of Identified Cholinergic, GABAergic, and Glutamatergic Neurons in the Pontomesencephalic Tegmentum of the Rat', *Journal of Neuroscience*, 34(13), pp. 4708–4727.

Cape, E. G. *et al.* (2000) 'Neurotensin-induced bursting of cholinergic basal forebrain neurons promotes gamma and theta cortical activity together with waking and paradoxical sleep.', *Journal of neuroscience*, 20(22), pp. 8452–8461.

Castel, M.-N. *et al.* (1989) 'Effects of ICV administration of neurotensin and analogs on EEG in rats', *Peptides*, 10, pp. 95–101.

Chung, S. *et al.* (2017) 'Identification of preoptic sleep neurons using retrograde labelling and gene profiling', *Nature*, 545(7655), pp. 477–481.

Clément, O. *et al.* (2011) 'Evidence that neurons of the sublaterodorsal tegmental nucleus triggering paradoxical (REM) sleep are glutamatergic', *Sleep*. Associated Professional Sleep Societies,LLC, 34(4). doi: 10.1093/sleep/34.4.419.

Clineschmidt, B. V and McGuffin, J. C. (1977) 'Neurotensin administered intracisternally inhibits responsiveness of mice to noxious stimuli.', *European journal of pharmacology*, 46(4), pp. 395–

396.
Crochet, S., Onoe, H. and Sakai, K. (2006) ‘A potent non-monoaminergic paradoxical sleep inhibitory system: a reverse microdialysis and single-unit recording study’, *European Journal of Neuroscience*, 24(5), pp. 1404–1412.
Dobner, P. R. *et al.* (2001) ‘Neurotensin-deficient mice show altered responses to antipsychotic drugs’, *Proceedings of the National Academy of Sciences*, 98(14), pp. 8048–8053.
Von Economo, C. (1930) ‘Sleep As a Problem of Localization’, *The Journal of Nervous and Mental Disease*, 71(march), pp. 249–259. doi: 10.1097/00005053-193003000-00001.
Erickson, E. T. M. *et al.* (2019) ‘Differential Role of Pontomedullary Glutamatergic Neuronal Populations in Sleep-Wake Control’, *Frontiers in Neuroscience*, 13, p. 755.
Fuller, P. *et al.* (2011) ‘Reassessment of the structural basis of the ascending arousal system’, *The Journal of Comparative Neurology*, 519(5), pp. 933–956. doi: 10.1002/cne.22559.
Furutani, N. *et al.* (2013) ‘Neurotensin Co-Expressed in Orexin-Producing Neurons in the Lateral Hypothalamus Plays an Important Role in Regulation of Sleep/Wakefulness States’, *PLoS ONE*, 8(4), p. e62391.
Hayashi, Y. *et al.* (2015) ‘Cells of a common developemtal origin or REM/non-REM sleep and wakefulness in Mice’, *Science*, 350(6263), pp. 957–962.
Iwasaki, K. *et al.* (2018) ‘Ablation of Central Serotonergic Neurons Decreased REM Sleep and Attenuated Arousal Response’, *Frontiers in Neuroscience*, 12, p. 12:535.
Jiang-Xie, L.-F. *et al.* (2019) ‘A Common Neuroendocrine Substrate for Diverse General Anesthetics and Sleep’, *Neuron*, in press. doi: https://doi.org/10.1016/j.neuron.2019.03.033.
Kompotis, K. *et al.* (2019) ‘Rocking Promotes Sleep in Mice through Rhythmic Stimulation of the Vestibular System’, *Current Biology*, 29(3), pp. 392–401.
Krenzer, M. *et al.* (2011) ‘Brainstem and Spinal Cord Circuitry Regulating REM Sleep and Muscle Atonia’, *PLoS ONE*, 6(10), p. e24998.
Kroeger, D. *et al.* (2018) ‘Galanin neurons in the ventrolateral preoptic area promote sleep and heat loss in mice’, *Nature Communications*, 9(1), p. 4129.
Leinninger, G. M. *et al.* (2011) ‘Leptin Action via Neurotensin Neurons Controls Orexin , the Mesolimbic Dopamine System and Energy Balance’, *Cell Metabolism*, 14(3), pp. 313–323.
Li, J. *et al.* (2016) ‘An obligatory role for neurotensin in high-fat-diet-induced obesity’, *Nature*, 533(7603), pp. 411–415.
Lu, J. *et al.* (2006) ‘A putative flip – flop switch for control of REM sleep’, *Nature*, 441(7093), pp. 589–594.
Ma, C. *et al.* (2019) ‘Sleep Regulation by Neurotensinergic Neurons in a Thalamo-Amygdala Circuit’, *Neuron*. doi: 10.1016/j.neuron.2019.05.015.
Machold, R. and Fishell, G. (2005) ‘Math1 Is Expressed in Temporally Discrete Pools of

Cerebellar Rhombic-Lip Neural Progenitors', *Neuron*, 48(1), pp. 17–24.
Madisen, L. *et al.* (2010) 'A robust and high-throughput Cre reporting and characterization system for the whole mouse brain', *Nature Neuroscience*, 13(1), pp. 133–140.
Moruzzi, G. and Magoun, H. W. (1949) 'Brain stem reticular formation and activation of the EEG', *Electroencephalography and Clinical Neurophysiology*, 1(4), pp. 455–473.
Naganuma, F. *et al.* (2019) 'Lateral hypothalamic neurotensin neurons promote arousal and hyperthermia', *PLOS Biology*, 17(3), p. e3000172.
Nakashiba, T. *et al.* (2008) 'Transgenic Inhibition of Synaptic Transmission Reveals Role of CA3 Output in Hippocampal Learning', *Science*, 319(5867), pp. 1260–1264.
Nauta, W. J. H. (1946) 'Hypothalamic regulation of sleep in rats; an experimental study', *Journal of Neurophysiology*, 9(4), pp. 285–316.
Rioux, F. *et al.* (1981) 'The hypotensive effect of centrally administered neurotensin in rats.', *European journal of pharmacology*, 69(3), pp. 241–247.
Saito, Y. C. *et al.* (2013) 'GABAergic neurons in the preoptic area send direct inhibitory projections to orexin neurons', *Frontiers in Neural Circuits*, 7(2), p. 192.
Sakai, K. (1988) 'Executive mechanisms of paradoxical sleep.', *Archives Italiennes de Biologie*, 126(4), pp. 239–257.
Sakai, K. (2015) 'Paradoxical (Rapid Eye Movement) sleep-on neurons in the laterodorsal pontine tegmentum in mice', *Neuroscience*, 310, pp. 455–471.
Sakai, K. (2018) 'Single unit activity of periaqueductal gray and deep mesencephalic nucleus neurons involved in sleep stage switching in the mouse', *European Journal of Neuroscience*, 47(9), pp. 1110–1126.
Sallanon, M. *et al.* (1989) 'Long-lasting insomnia induced by preoptic neuron lesions and its transient reversal by muscimol injection into the posterior hypothalamus in the cat', *Neuroscience*, 32(3), pp. 669–683.
Sapin, E. *et al.* (2009) 'Localization of the Brainstem GABAergic Neurons Controlling Paradoxical (REM) Sleep', *PLoS ONE*, 4(1), p. e4272.
Sastre, J.-P., Sakai, K. and Jouvet, M. (1981) 'Are the gigantocellular tegmental field neurons responsible for paradoxical sleep?', *Brain Research*, 229(1), pp. 147–161. doi: 10.1016/0006-8993(81)90752-6.
Schroeder, L. E. *et al.* (2019) 'Mapping the populations of neurotensin neurons in the male mouse brain', *Neuropeptides*, 76, p. 101930.
Sherin, J. E. *et al.* (1996) 'Activation of ventrolateral preoptic neurons during sleep.', *Science*, 271(5246), pp. 216–219.
Siegel, J. M. *et al.* (1996) 'The echidna Tachyglossus aculeatus combines REM and non-REM aspects in a single sleep state: implications for the evolution of sleep.', *The Journal of*

neuroscience : the official journal of the Society for Neuroscience, 16(10), pp. 3500–3506.
Valencia Garcia, S. *et al.* (2016) 'Genetic inactivation of glutamate neurons in the rat sublaterodorsal tegmental nucleus recapitulates REM sleep behaviour disorder', *Brain*, 140(2), pp. 414–428.
Vanni-Mercier, G. *et al.* (1989) 'Mapping of cholinoceptive brainstem structures responsible for the generation of paradoxical sleep in the cat.', *Archives Italiennes de Biologie*, 127(3), pp. 133–164.
Wang, V. Y., Rose, M. F. and Zoghbi, H. Y. (2005) 'Math1 expression redefines the rhombic lip derivatives and reveals novel lineages within the brainstem and cerebellum', *Neuron*, 48(1), pp. 31–43.
Weber, F. *et al.* (2015) 'Control of REM sleep by ventral medulla GABAergic neurons', *Nature*, 526(7573), pp. 435–438.
Weber, F. *et al.* (2018) 'Regulation of REM and Non-REM Sleep by Periaqueductal GABAergic Neurons', *Nature Communications*, 9(1), p. 354.
Weber, F. and Dan, Y. (2016) 'Circuit-based interrogation of sleep control.', *Nature*, 538(7623), pp. 51–59.
Yasuda, K. *et al.* (2017) 'Schizophrenia-like phenotypes in mice with NMDA receptor ablation in intralaminar thalamic nucleus cells and gene therapy-based reversal in adults', *Translational Psychiatry*, 7(2), p. e1047.
Zhang, Z. *et al.* (2015) 'Neuronal ensembles sufficient for recovery sleep and the sedative actions of α2 adrenergic agonists', *Nature Neuroscience*, 18(4), pp. 553–561.

Figure legend

Fig. 1 Identification of *Nts* as a molecular marker for a subset of neurons in the SubLDT.

A, Fluorescent *in situ* hybridization (ISH) revealing that a subset of neurons in the SubLDT strongly expresses *Nts*. (Scale bar 0.5 mm, Yellow; *Nts* (ISH) Blue; DAPI (4', 6-diamidino-2-phenylindole))

B-C, Overlap between *Nts* expression and *Atoh1* lineage neurons. (Scale bar; 50 μm, magenta; *Nts* (ISH), Green; *Atoh1*-EYFP (IHC)) Data represent mean ± SEM. n=6 sections/group, obtained from 3 mice.

D-G, Co-expression analysis of GCaMP6s (*Nts-Cre;* AAV-*hSyn-flex-GCaMP6s*) with *Nts* (ISH) or Chat (IHC) (D,G), or Rpl10a-GFP (*Nts-Cre; Rosa-loxP-STOP-loxP-Rpl10a-GFP*) with *Vglut2* (ISH) or *Vgat* (ISH) (E,F) in SubLDT. Data represent mean ± SEM. n=8 sections for D and G, and n=4 sections for E and F, obtained from 4 mice. (Scale bar: 50 μm, Green: GCaMP6s or Rpl10a-GFP, Magenta: *Nts*, *Vglut2*, *Vgat*, or Chat, respectively)

Fig. 2 Chemogenetic activation of *Nts*-neurons increased NREM sleep

A, AAV encoding Cre inducible hM3Dq-mCherry were microinjected into the SubLDT of *Nts-Cre* mice.

B, Cre-driven transgene expression was detected in SubLDT. Note that strong signals were detected from both the soma and neurites, resulting in a broader signal compared with that shown in Figure 1A. (Scale bar: 0.5mm, Yellow: hM3Dq-mCherry, Blue: DAPI)

C, Heatmaps showing the area of AAV transfection. The average number of cells expressing AAV-derived transgene per hemisphere is indicated below each section.

D, CNO administration activated c-fos expression. (Scale bar: 50 μm. Magenta: hM3Dq-mCherry, Green: c-fos). Data represent mean ± SEM. n=5 sections, obtained from 3 mice. ***P < 0.001 [unpaired Student's t-test].

E, Representative traces of EEG and EMG signals, hypnograms, and delta power after administration of saline or CNO.

F, Chemogenetic activation of *Nts*-neurons increased NREM sleep at the expense of both wakefulness and REM sleep. Saline or CNO (1.5 mg/kg) was administered at ZT5. Horizontal axes indicate time after drug administration. Data represent mean ± SEM. n=10 mice/group. *P <0.05; ** †† ‡‡P < 0.005; *** ††† ‡‡‡P < 0.001 [two-way repeated measures ANOVA followed by Bonferroni's test; † and ‡ indicate significant main effect of intervention and significant interaction between intervention and time, respectively, in two-way repeated measures ANOVA, and * indicates significance in Bonferroni's test].

G-I, Sleep architecture in the 2h after saline or CNO (1.5 mg/kg) administration. Data represent mean ± SEM. n=10 mice. **P < 0.005; ***P < 0.001 [paired Student's t-test].

J, Normalized EEG power spectrum in each state. Data represent mean ± SEM. n=10 mice except for REM after CNO administration, n=9 mice in REM after CNO administration (one mouse did not exhibit REM sleep after CNO administration). * † ‡P <0.05; **P < 0.005; ***P < 0.001 [two-way repeated measures ANOVA followed by Bonferroni's test; † and ‡ indicate significant main effect of intervention and significant interaction between intervention and frequency, respectively, in two-way repeated measures ANOVA, and * indicates significance in Bonferroni's test (same in O)]

K, The amount of each vigilance state in the 2h after saline or CNO (1.5 mg/kg) administration. Here, administration was performed in the dark phase (ZT17). Data represent mean ± SEM. n=3 mice. *P <0.05 [paired Student's t-test]

Fig. 3 Additional analyses of the effect of chemogenetic activation of *Nts*-neurons in the SubLDT

A-C, Analysis of the effect of chemogenetic activation of *Nts*-neurons on a longer period (24 hours after saline or CNO (1.5 mg/kg) administration). Saline or CNO (1.5 mg/kg) was administered at ZT5. Horizontal axes indicate time after drug administration. Data represent mean ± SEM. n=5

mice/group. * ‡P <0.05; ** †† ‡‡P < 0.005; ‡‡‡P < 0.001 [two-way repeated measures ANOVA followed by Bonferroni's test; † and ‡ indicate significant main effect of intervention and significant interaction between intervention and time, respectively, in two-way repeated measures ANOVA, and * indicates significance in Bonferroni's test (same for D-F)].

D, CNO (1.5 mg/kg) administration at ZT5 did not alter vigilance states in mice injected with the control virus (AAV-*hSyn-DIO-mCherry*). Data represent mean ± SEM. n=4 mice/group. [two-way repeated measures ANOVA followed by Bonferroni's test]

Fig. 4 Functional inactivation of *Nts*-neurons decreased NREM sleep

A, AAV encoding Cre inducible GFP-T2A-TeTx was microinjected into the SubLDT of *Nts-Cre* mice.

B-C, Cre-driven transgene expression was detected in the SubLDT. (Scale bar: 0.5 mm, Yellow: GFP, Blue: DAPI)

D, TeTx expression in *Nts*-neurons reduced NREM sleep. Data represent mean ± SEM. n=7 mice in mCherry group, n=9 mice in TeTx group. * †P <0.05; ** ‡‡P < 0.005, ***P < 0.001 [Bonferroni's test for 24h, two-way repeated measures ANOVA followed by Bonferroni's test for the light and dark phase comparison; † and ‡ indicate significant main effect of intervention and significant interaction between intervention and period of the day, respectively, in two-way repeated measures ANOVA, and * indicates significance in Bonferroni's test including 24h data.]

E, Amount of each vigilance state every hour over 24h in mice injected with mCherry (AAV-*hSyn-DIO-mCherry*) or TeTx (AAV-*hSyn-DIO-GFP-T2A-TeTx*). Data represent mean ± SEM. n=7 mice in mCherry group, n=9 mice in TeTx group. †P < 0.05 [two-way repeated measures ANOVA followed by Bonferroni's test; † and ‡ indicate significant main effect of intervention and significant interaction between intervention and time, respectively, in two-way repeated measures ANOVA, and * indicates significance in Bonferroni's test].

F-G, Sleep architecture during 24h, light phase, or dark phase, were analyzed. Data represent mean ± SEM. n=7 mice in mCherry group, n=9 mice in TeTx group. † ‡P <0.05; †† ‡‡P < 0.005; ***P < 0.001 [Bonferroni's test for 24h, two-way repeated measures ANOVA followed by Bonferroni's test for the light and dark phase comparison; † and ‡ indicate significant main effect of intervention and significant interaction between intervention and period of the day, respectively, in two-way repeated measures ANOVA, and * indicates significance in Bonferroni's test including 24h data]

H, Normalized EEG power spectrum in each state. Data represent mean ± SEM. n=7 mice in mCherry group, n=9 mice in TeTx group. † ‡P <0.05 [two-way repeated measures ANOVA followed by Bonferroni's test].

Fig. 5 Projection targets of SubLDT *Nts*-neurons

A, AAV encoding Cre inducible tdTomato-T2A-synaptophysin-GFP was microinjected into the SubLDT of *Nts-Cre* mice.

B, Cre-driven transgene (tdTomato) expression was detected in the SubLDT. (Scale bar: 0.5 mm (Left figure), 50 μm (Right figure), Yellow: tdTomato (IHC), Blue: DAPI)

C-D, Cre-driven synaptophysin-GFP, which localizes in pre-synaptic structures, was detected in the dDpMe, lPAG, and MVe, in close proximity to somata positive for *Nts*. (Scale bar: 20 μm. Magenta: *Nts* (ISH), Green: synaptophysin-GFP (IHC), white: tdTomato (IHC)) (dDpMe: dorsal deep mesencephalic nucleus, lPAG: lateral part of the periaqueductal gray, MVe: medial vestibular nucleus)

E, Distribution of *Nts*-neurons in the dDpMe, lPAG, and MVe visualized using *Nts-Cre; Rosa26-CAG-LSL-Rpl10a-GFP* mice. (Scale bar: 0.5mm. Blue: DAPI, Yellow: Rpl10a-GFP)

Fig. 6 Identification of *Nts*-neurons that regulate sleep in the dDpMe, lPAG, and MVe.

A-B, F-G, K-L, AAV encoding Cre inducible hM3Dq-mCherry was microinjected into the dDpMe, lPAG, and MVe of *Nts-Cre* mice, and Cre-driven transgene expression was confirmed in each brain area. Note that strong signals were detected from both the somata and neurites, resulting in a broader signal compared with that shown in Figure 5E. (Scale bar: 0.5mm, Yellow: hM3Dq-mCherry, Blue: DAPI)

C, H, M, Heatmaps showing the area of AAV transfection. The average number of cells expressing AAV transgene per hemisphere is indicated below each section.

D, I, N, Representative traces of EEG and EMG signals, hypnograms, and delta power after administration of saline or CNO.

E, J, O, Chemogenetic activation of *Nts*-neurons in each brain area increased NREM sleep at the expense of both wakefulness and REM sleep. Saline or CNO (1.5 mg/kg) was administered at ZT5. Horizontal axes indicate time after drug administration. Data represent mean ± SEM. n=6 mice for dDpMe, 5 mice for lPAG and MVe, respectively. * † ‡P <0.05; ** †† ‡‡P < 0.005; *** ‡‡‡P < 0.001 [two-way repeated measures ANOVA followed by Bonferroni's test; † and ‡ indicate significant main effect of intervention and significant interaction between intervention and time, respectively, in two-way repeated measures ANOVA, and * indicates significance in Bonferroni's test.]

Fig. 7 Histologic analyses of co-expressed factors within *Nts*-neurons in dDpMe, lPAG, and MVe.

A, E, I, CNO administration activated c-fos expression in *Nts*-neurons in dDpMe (A), lPAG (E), and MVe (I). (Scale bar: 50 μm. Magenta: hM3Dq-mCherry, Green: c-fos) Data represent mean ± SEM. n=6 sections, obtained from 3 mice. ***P < 0.001 [unpaired Student's t-test]

B-D, F-H, J-L, Co-expression analysis of hM3Dq-mCherry with *Nts* (ISH), *Vglut2* (ISH), or *Vgat* (ISH) in dDpMe (B-D), lPAG (F-H), and MVe (J-L). Data represent mean ± SEM. n=9 sections, obtained from 3 mice. (Scale bar: 50 μm, Green: hM3Dq-mCherry, Magenta: *Nts*, *Vglut2*, or *Vgat*, respectively)

Fig. 8 Additional analyses on the effect of manipulation of *Nts*-neurons in dDpMe, lPAG, and MVe.

A-C, F-H, K-M, Sleep architecture in the 2h after saline or CNO (1.5 mg/kg) administration at ZT5 in the dDpMe (A-C), lPAG (F-H), and MVe (K-M). Data represent mean ± SEM. n=6 mice in dDpMe group, 5 mice in lPAG and MVe groups. *P <0.05; **P < 0.005; ***P < 0.001 [paired Student's t-test].

D, I, N, Normalized EEG power spectrum in each state. Data represent mean ± SEM. n=6 mice except for REM after CNO administration, n=5 mice in REM after CNO administration (D), n=5 mice except for REM after CNO administration, n=4 mice in REM after CNO administration (I, N). (For each group, one mouse did not exhibit REM sleep after CNO administration) * †P <0.05; **P< 0.005; *** ‡‡‡P< 0.001 [two-way repeated measures ANOVA followed by Bonferroni's test; † and ‡ indicate significant main effect of intervention and significant interaction between intervention and frequency, respectively, in two-way repeated measures ANOVA, and * indicates significance in Bonferroni's test]

E, J, O, The amount of each vigilance state in the 2h after saline or CNO (1.5 mg/kg) administration in the dDpMe (E), lPAG (J), and MVe (O). Here, administration was performed in the dark phase (ZT17). Data represent mean ± SEM. n=6 mice in dDpMe, 3 mice in the lPAG, and 5 mice in MVe. *P <0.05 [paired Student's t-test]

Fig. 9 *Nts*-neurons in the lPAG and MVe were activated by sleep deprivation.

A-C, Comparison of c-fos expression in the *Nts*-neurons in SubLDT, dDpMe, lPAG, and MVe of *Nts-Cre; Rosa-loxP-STOP-loxP-Rpl10a-GFP* mice under conditions summarized in (P). Data represent mean ± SEM. n=6 sections, obtained from 3 mice. (Scale bar: 50 μm, Green: Rpl10a-GFP, Magenta: c-fos). * †P <0.05; *** †††P< 0.001 [one-way ANOVA followed by Tukey's test; † indicates significant effect of condition in one-way ANOVA, and * indicates significance in Tukey's test]

Fig. 10 Neurotensin peptide infusion induced a behaviorally quiescent state with cortical slow wave activity.

A, For intracerebroventricular (ICV) infusion of neurotensin, a cannula was placed in the fourth ventricle of WT mice.

B, Representative EEG/EMG trace after saline or peptide (20 ng) infusion. Peptide infusion induced a behaviorally quiescent state with cortical slow wave activity, characterized by slow wave (0.5-4.0Hz) dominant EEG and EMG amplitudes lower than natural NREM sleep. In subsequent panels, this behaviorally quiescent state with cortical slow wave activity is summarized together with natural NREM sleep as 'NREM(-like).

C, Amount of each vigilance state following saline or peptide infusion. Administration was performed at ZT5. Horizontal axes indicate time after infusion of the reagents. Data represent the mean ± SEM. n=5 mice/group. * ‡P <0.05; **P< 0.005; ‡‡‡P< 0.001 [two-way repeated measures ANOVA followed by Bonferroni's test; † and ‡ indicate significant main effect of intervention and significant interaction between intervention and time, respectively, in two-way repeated measures ANOVA, and * indicates significance in Bonferroni's test].

D-F, Sleep architecture in the 2h after infusion. Data represent mean ± SEM. n=5 mice/group. *P <0.05; [paired Student's t-test].

G, Normalized EEG power spectrum in each state. Data represent mean ± SEM. n=5 mice/group in awake and NREM(-like). n=4 mice/group in REM. (In each group, one mouse did not exhibit REM sleep). *P <0.05; *** ‡‡‡P< 0.001 [two-way repeated measures ANOVA followed by Bonferroni's test; ‡ indicates significant interaction between intervention and frequency, and * indicates significance in Bonferroni's test.].

H, Amount of each vigilance state in the 2h after infusion. Administration was performed at ZT17. Horizontal axes indicate time after administration. Data represent the mean ± SEM. n=5 mice/group. *P <0.05; **P < 0.005 [paired Student's t-test].

Fig. 11 Neurotensin-deficient mice (*Nts*$^{-/-}$) showed increased REM sleep

A, Neurotensin-deficient mice (*Nts*$^{-/-}$) showed increased REM sleep and ratio of REM sleep to total sleep compared to WT littermates (*Nts*$^{+/+}$). Each graph indicates total amount of awake, NREM, REM, or REM/total sleep ratio over 24 h, light phase, or dark phase, respectively. Data represent mean ± SEM. n=9 mice in *Nts*$^{+/+}$ group, n=12 mice in *Nts*$^{-/-}$ group. ** ††P < 0.005 [Bonferroni's test for 24h, two-way repeated measures ANOVA followed by Bonferroni's test for the light and dark phase comparison; † indicates significant main effect of genotype in two-way repeated measures ANOVA, and * indicates significance in Bonferroni's test including 24h data.]

B, Amount of each vigilance state every hour over 24h in mice deficient for neurotensin (*Nts*$^{-/-}$) or WT littermates (*Nts*$^{+/+}$). Data represent mean ± SEM. n=9 mice in the *Nts*$^{+/+}$ group, n=12 mice in the *Nts*$^{-/-}$ group. ‡P <0.05; ††P < 0.01 [two-way repeated measures ANOVA followed by Bonferroni's test; † and ‡ indicate significant main effect of genotype and significant interaction between genotype and time, respectively, in two-way repeated measures ANOVA, and * indicates significance in Bonferroni's test].

C-D, Sleep architecture during 24h, light phase, or dark phase was analyzed. Data represent mean ± SEM. n=9 mice in the *Nts*$^{+/+}$ group, n=12 mice in the *Nts*$^{-/-}$ group. [Bonferroni's test for 24h, two-way repeated measures ANOVA followed by Bonferroni's test for the light and dark phase comparison].

E, Normalized EEG power spectrum in each states. Data represent mean ± SEM. n=9 mice in *Nts*$^{+/+}$ group, n=11 mice in *Nts*$^{-/-}$ group. (One mouse in the *Nts*$^{-/-}$ group was excluded due to contamination by large noise). * ‡P <0.05; ** ††P< 0.005; *** ††† ‡‡‡P< 0.001 [two-way repeated measures ANOVA followed by Bonferroni's test; † and ‡ indicate significant main effect of genotype and significant interaction between genotype and frequency, respectively, in two-way repeated measures ANOVA, and * indicates significance in Bonferroni's test.].

Fig.1

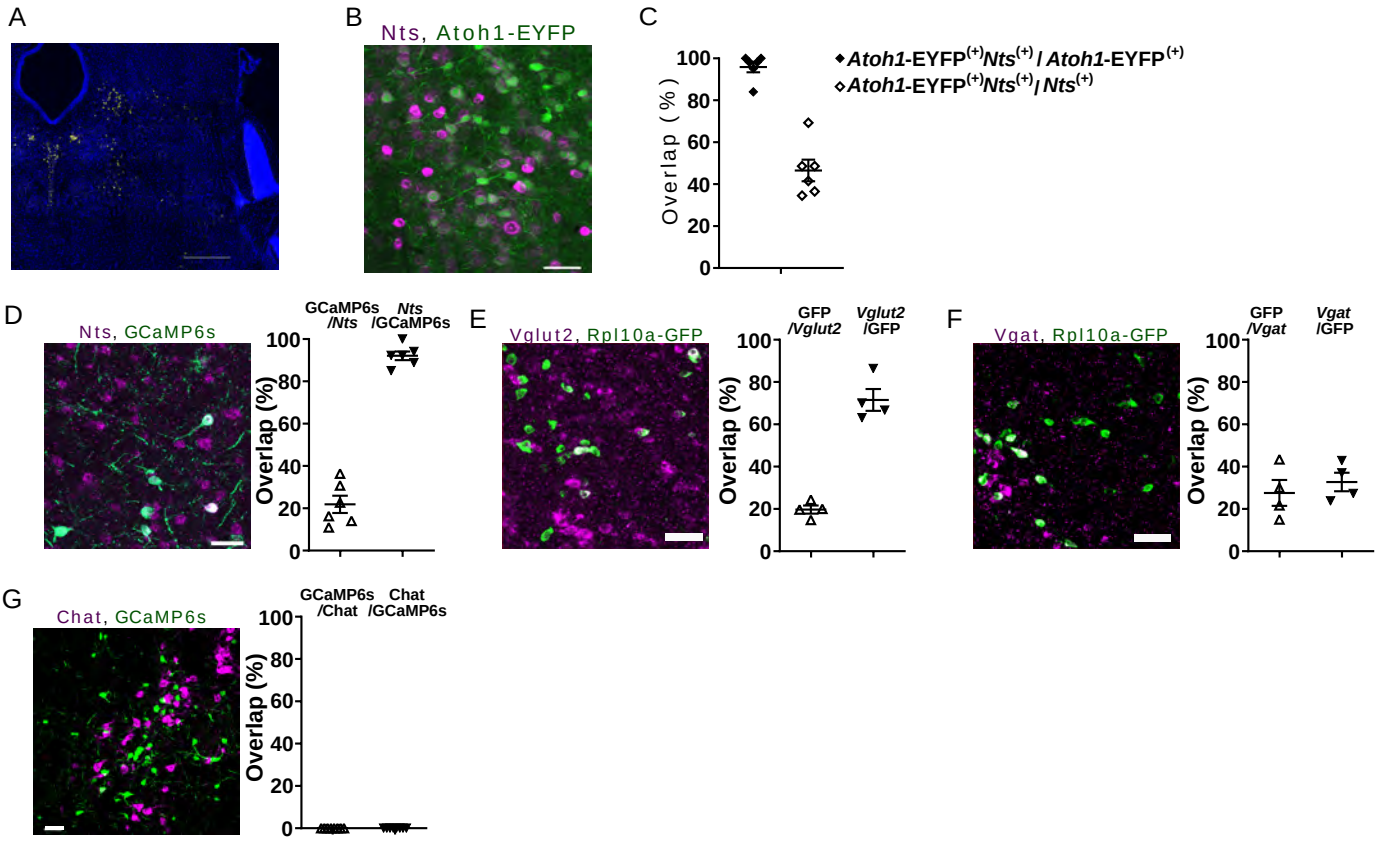
A
B
Nts, Atoh1-EYFP
C
Overlap (%)
Atoh1-EYFP(+)Nts(+) / Atoh1-EYFP(+)
Atoh1-EYFP(+)Nts(+) / Nts(+)
D
Nts, GCaMP6s
GCaMP6s /Nts
Nts /GCaMP6s
Overlap (%)
E
Vglut2, Rpl10a-GFP
GFP /Vglut2
Vglut2 /GFP
F
Vgat, Rpl10a-GFP
GFP /Vgat
Vgat /GFP
G
Chat, GCaMP6s
GCaMP6s /Chat
Chat /GCaMP6s

Fig.2

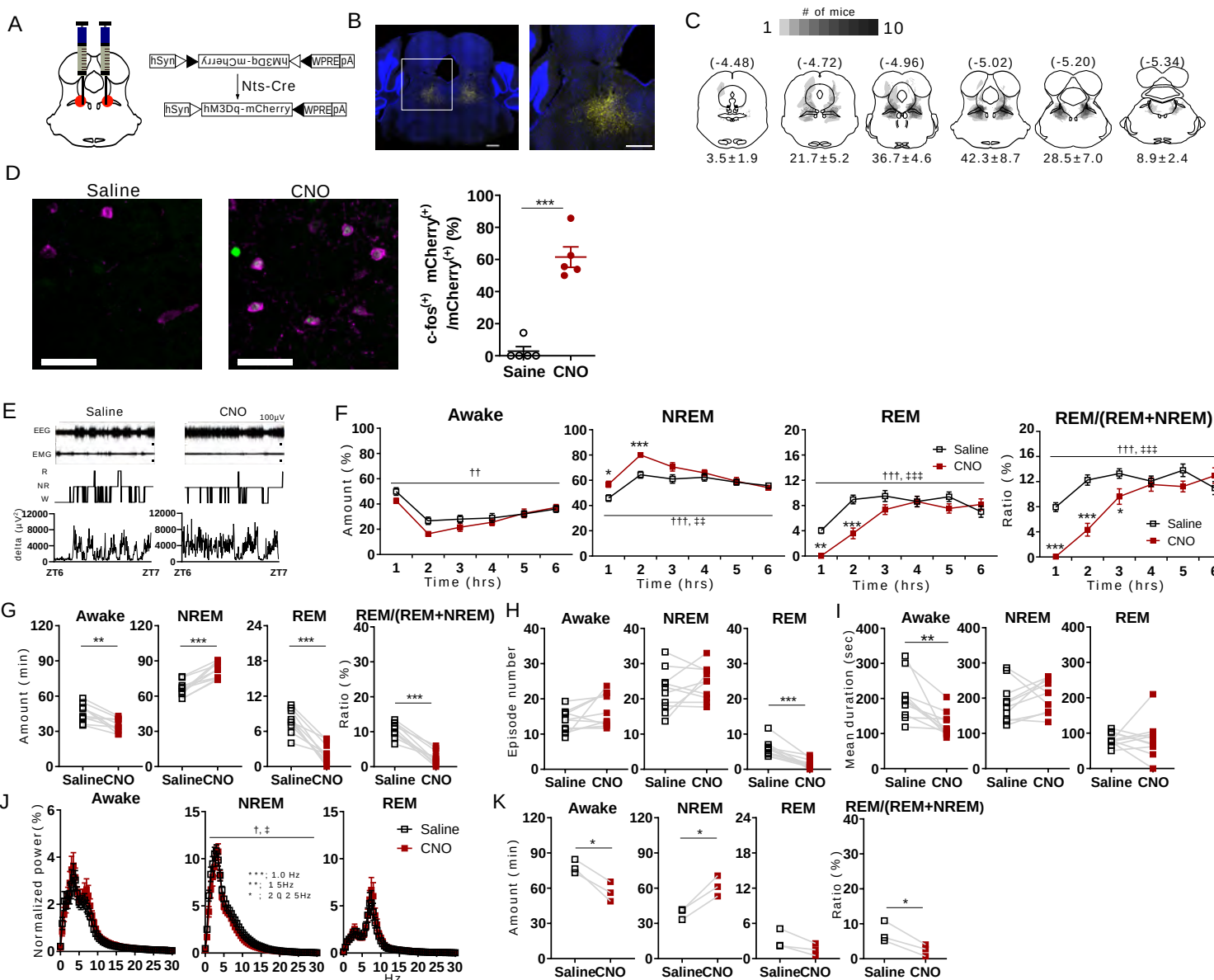
A
hSyn
hM3Dq-mCherry
WPRE
pA
Nts-Cre
B
C
# of mice
1
10
(-4.48)
(-4.72)
(-4.96)
(-5.02)
(-5.20)
(-5.34)
3.5±1.9
21.7±5.2
36.7±4.6
42.3±8.7
28.5±7.0
8.9±2.4
D
Saline
CNO
c-fos(+) mCherry(+) /mCherry(+) (%)
Saine CNO
E
Saline
CNO
EEG
EMG
R
NR
W
delta (μV²)
ZT6
ZT7
F
Awake
NREM
REM
REM/(REM+NREM)
Amount (%)
Ratio (%)
Time (hrs)
Saline
CNO
G
Amount (min)
SalineCNO
H
Episode number
I
Mean duration (sec)
J
Normalized power(%)
Hz
K
Amount (min)
Ratio (%)

Fig.3

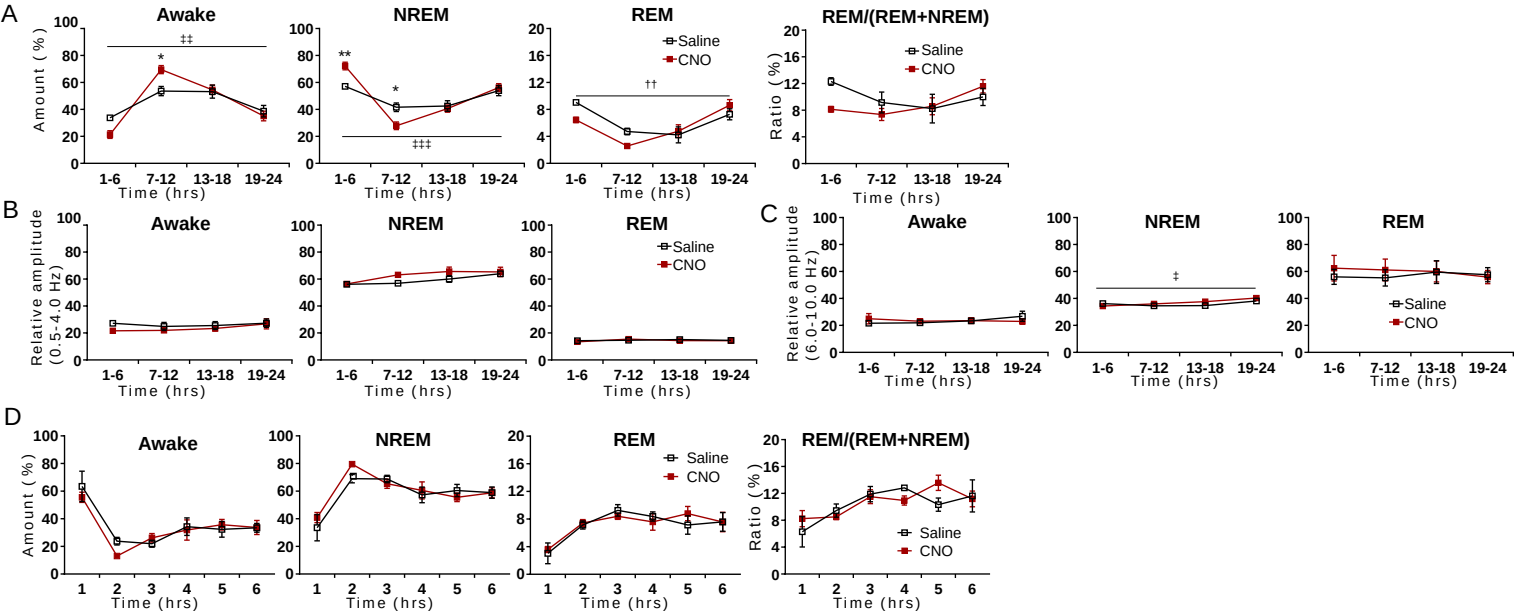
A
Awake
NREM
REM
REM/(REM+NREM)
Amount (%)
Ratio (%)
Saline
CNO
Time (hrs)
1-6
7-12
13-18
19-24
B
Relative amplitude (0.5-4.0 Hz)
C
Relative amplitude (6.0-10.0 Hz)
D

Fig.4

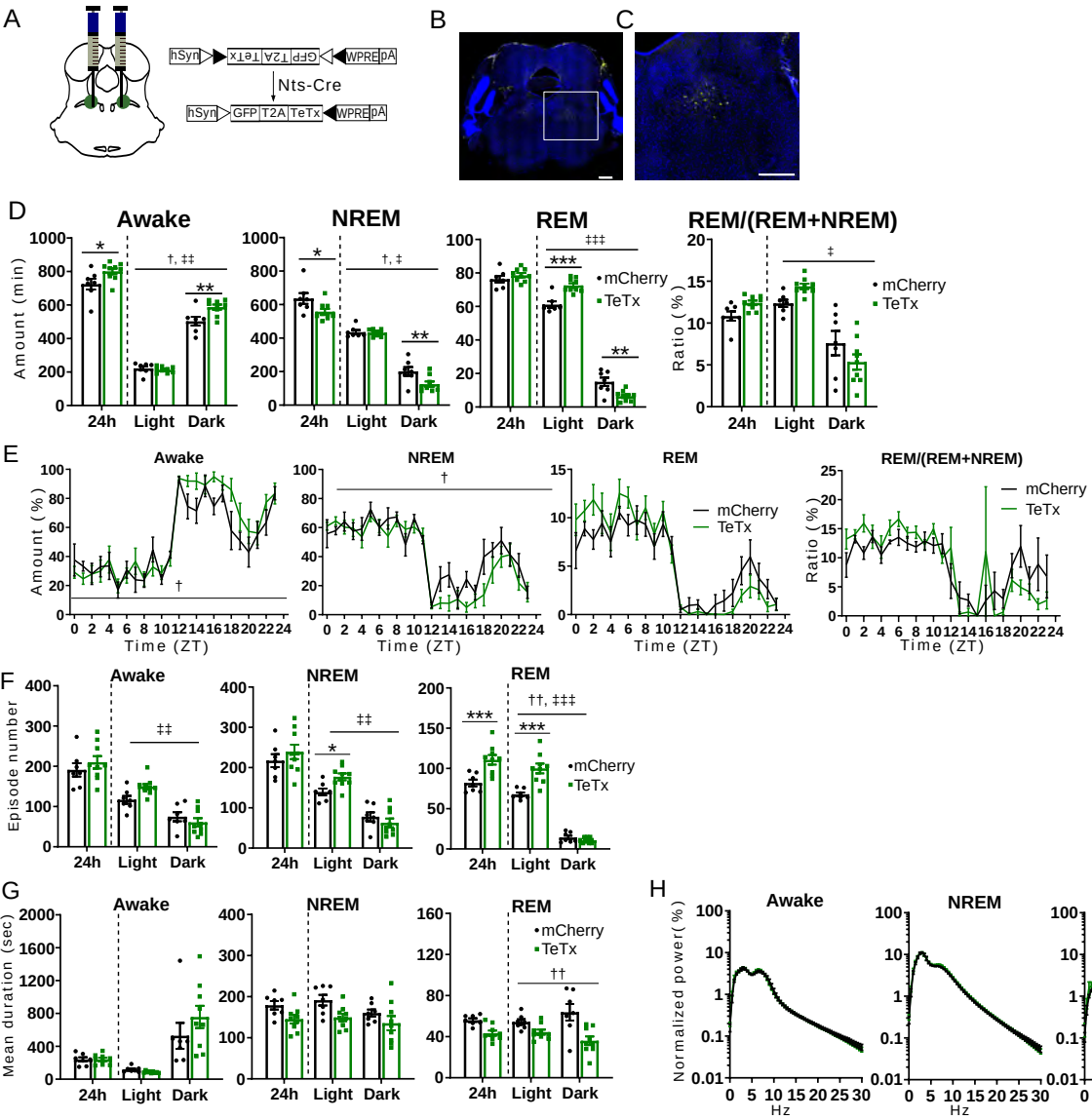
A
hSyn
GFP T2A TeTx
WPRE pA
Nts-Cre
B
C
D
Awake
NREM
REM
REM/(REM+NREM)
Amount (min)
Ratio (%)
24h Light Dark
mCherry
TeTx
E
Amount (%)
Time (ZT)
F
Episode number
G
Mean duration (sec)
H
Normalized power (%)
Hz

Fig.5

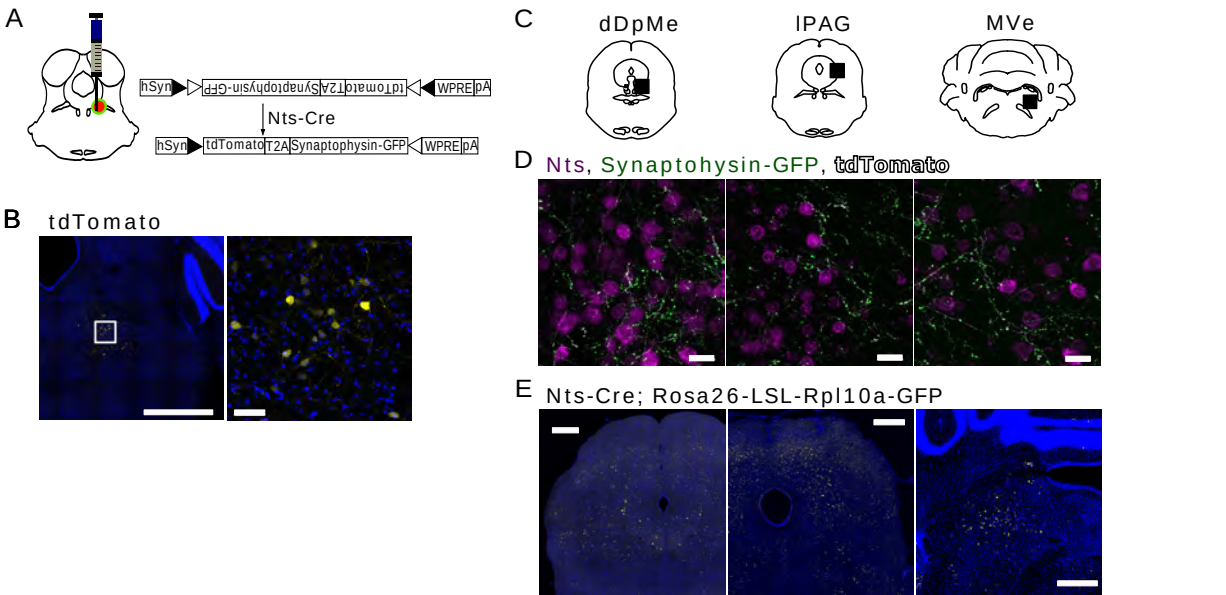
A
hSyn
tdTomato T2A Synaptophysin-GFP
WPRE pA
Nts-Cre
B
tdTomato
C
dDpMe
lPAG
MVe
D
Nts, Synaptophysin-GFP, tdTomato
E
Nts-Cre; Rosa26-LSL-Rpl10a-GFP

Fig.6

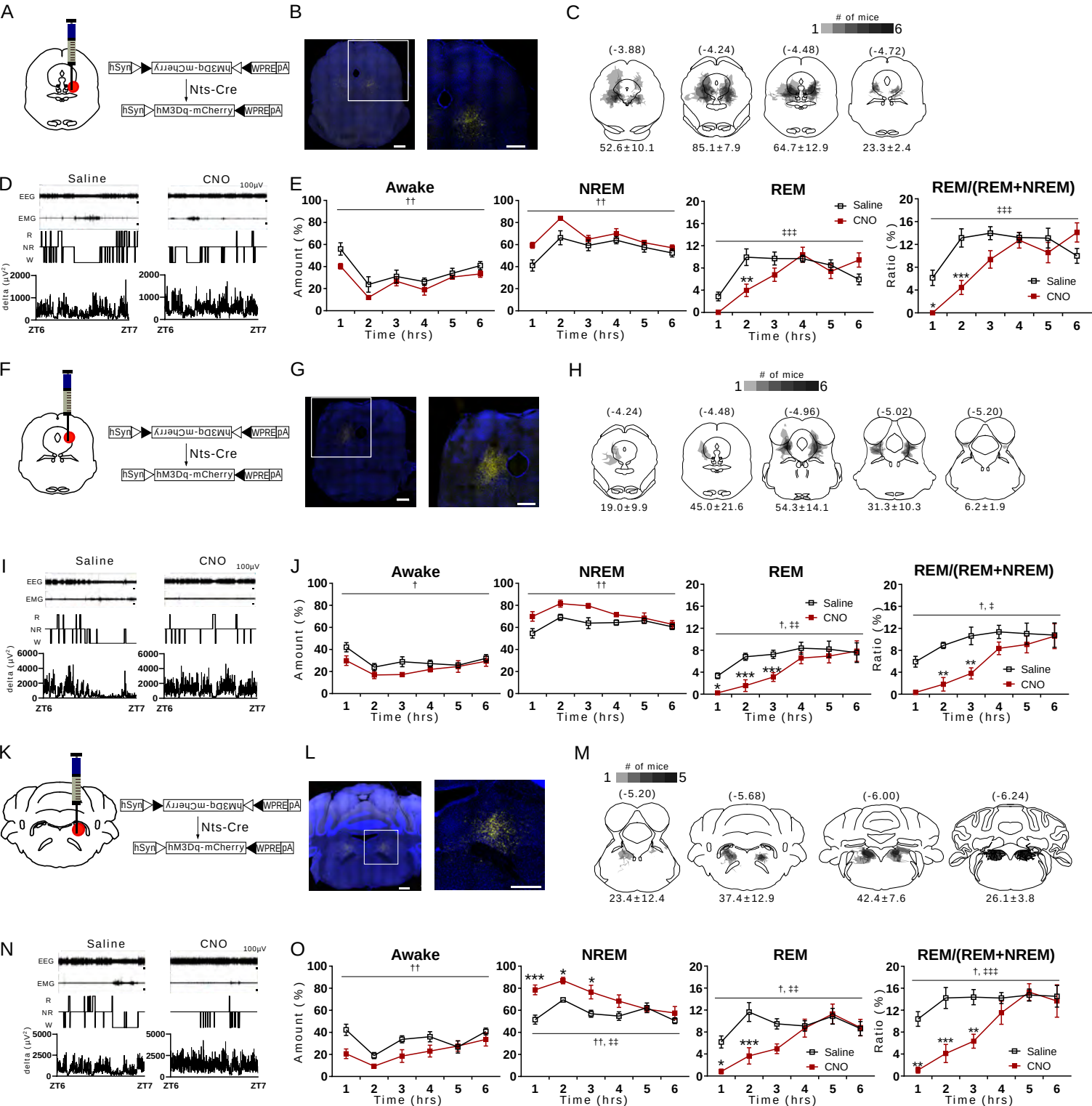
A
hSyn
hM3Dq-mCherry
WPRE
pA
Nts-Cre
B
C
# of mice
1
6
(-3.88)
(-4.24)
(-4.48)
(-4.72)
52.6±10.1
85.1±7.9
64.7±12.9
23.3±2.4
D
Saline
CNO
100μV
EEG
EMG
R
NR
W
delta (μV²)
ZT6
ZT7
E
Awake
NREM
REM
REM/(REM+NREM)
Amount (%)
Ratio (%)
Time (hrs)
Saline
CNO
F
G
H
(-4.24)
(-4.48)
(-4.96)
(-5.02)
(-5.20)
19.0±9.9
45.0±21.6
54.3±14.1
31.3±10.3
6.2±1.9
I
J
K
L
M
(-5.20)
(-5.68)
(-6.00)
(-6.24)
23.4±12.4
37.4±12.9
42.4±7.6
26.1±3.8
N
O

Fig.7

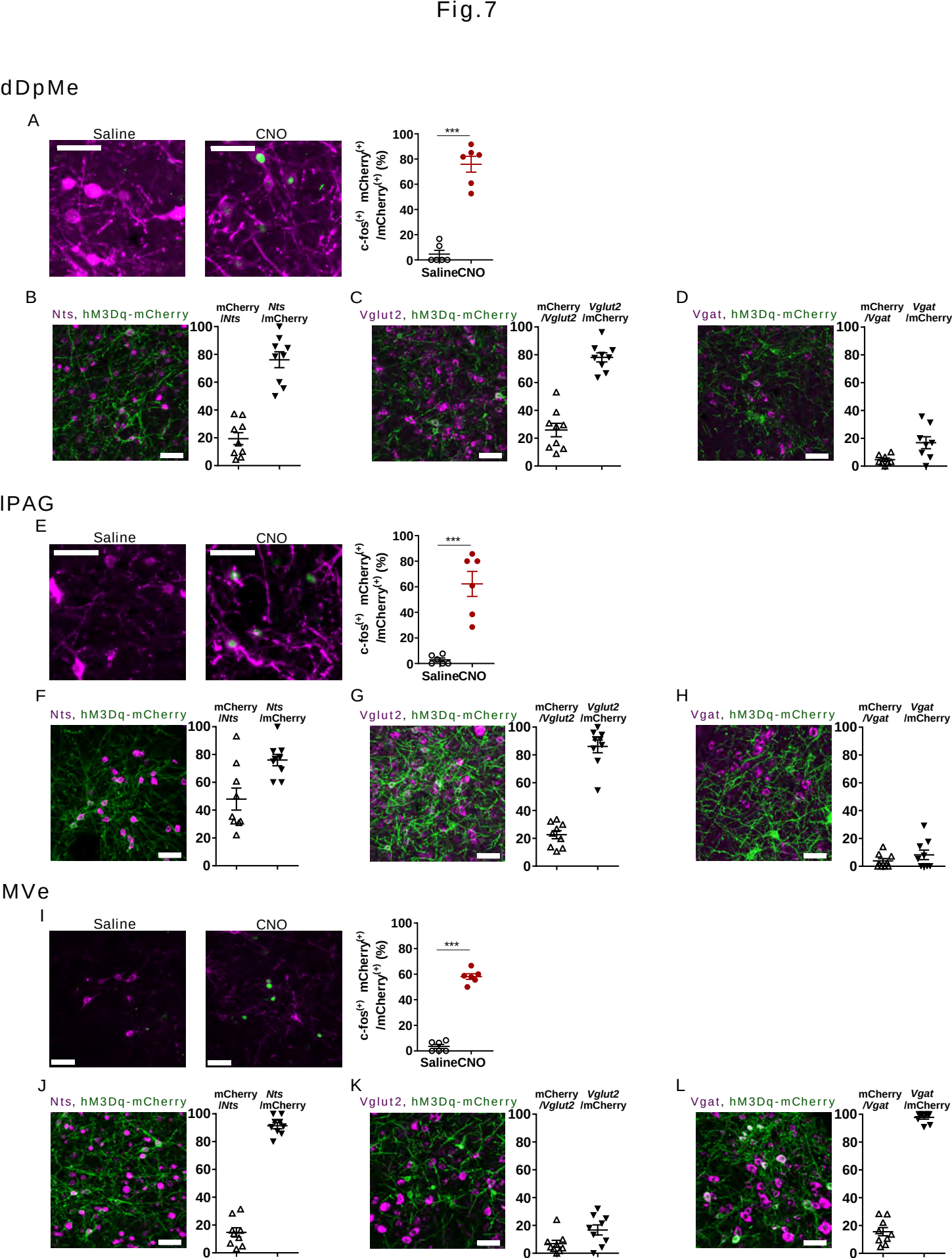
dDpMe
A
Saline
CNO
***
c-fos(+) mCherry(+) /mCherry(+) (%)
SalineCNO
B
Nts, hM3Dq-mCherry
mCherry /Nts
Nts /mCherry
C
Vglut2, hM3Dq-mCherry
mCherry /Vglut2
Vglut2 /mCherry
D
Vgat, hM3Dq-mCherry
mCherry /Vgat
Vgat /mCherry
lPAG
E
Saline
CNO
***
c-fos(+) mCherry(+) /mCherry(+) (%)
SalineCNO
F
Nts, hM3Dq-mCherry
mCherry /Nts
Nts /mCherry
G
Vglut2, hM3Dq-mCherry
mCherry /Vglut2
Vglut2 /mCherry
H
Vgat, hM3Dq-mCherry
mCherry /Vgat
Vgat /mCherry
MVe
I
Saline
CNO
***
c-fos(+) mCherry(+) /mCherry(+) (%)
SalineCNO
J
Nts, hM3Dq-mCherry
mCherry /Nts
Nts /mCherry
K
Vglut2, hM3Dq-mCherry
mCherry /Vglut2
Vglut2 /mCherry
L
Vgat, hM3Dq-mCherry
mCherry /Vgat
Vgat /mCherry

Fig.8

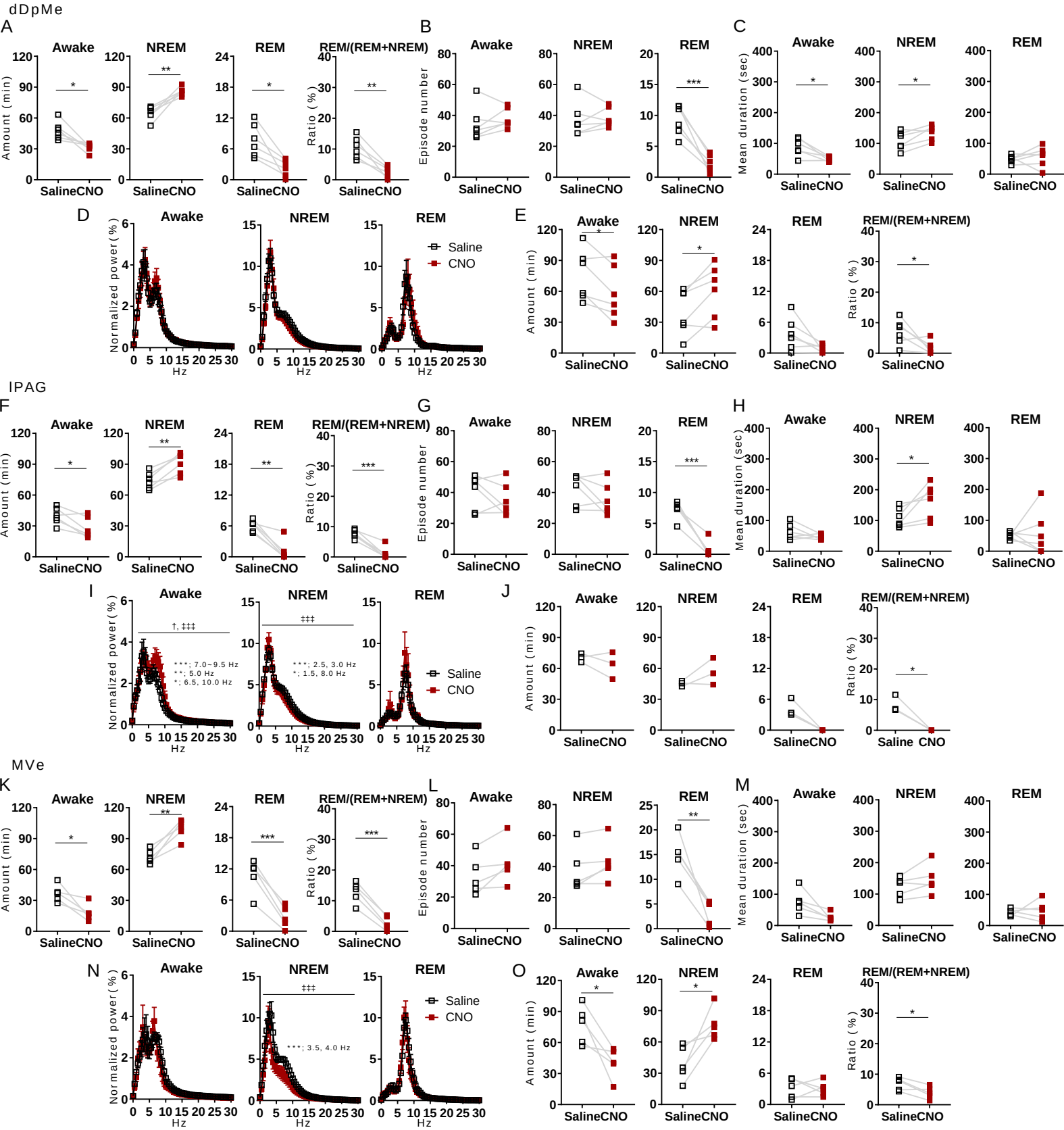
dDpMe
A
Awake
NREM
REM
REM/(REM+NREM)
Amount (min)
Ratio (%)
SalineCNO
B
Episode number
C
Mean duration (sec)
D
Normalized power (%)
Hz
Saline
CNO
E
IPAG
F
G
H
I
†, ‡‡‡
‡‡‡
***; 7.0–9.5 Hz
**; 5.0 Hz
*; 6.5, 10.0 Hz
***; 2.5, 3.0 Hz
*; 1.5, 8.0 Hz
J
Saline CNO
MVe
K
L
M
N
***; 3.5, 4.0 Hz
O

Fig.9

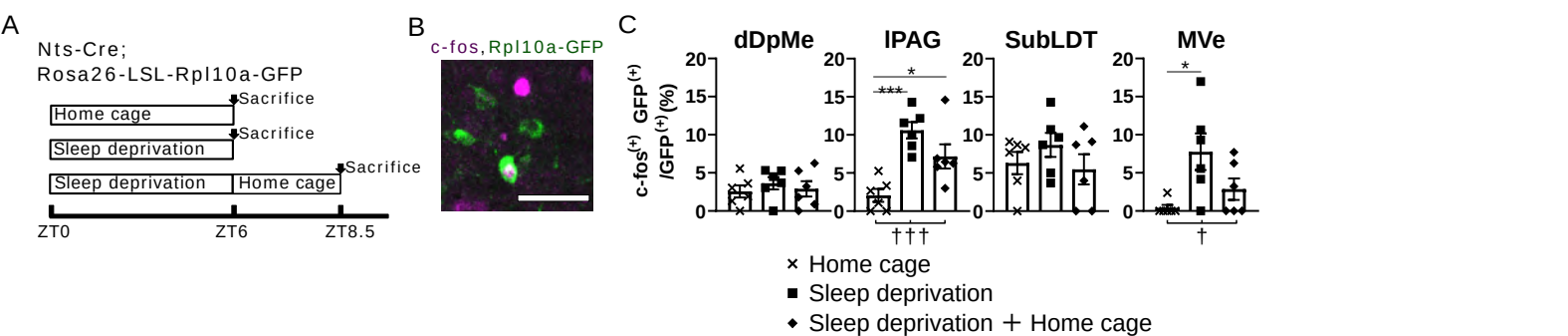
A
Nts-Cre;
Rosa26-LSL-Rpl10a-GFP
Sacrifice
Home cage
Sleep deprivation
Sleep deprivation
Home cage
ZT0
ZT6
ZT8.5
B
c-fos, Rpl10a-GFP
C
dDpMe
lPAG
SubLDT
MVe
c-fos(+) GFP(+) /GFP(+) (%)
Home cage
Sleep deprivation
Sleep deprivation + Home cage

Fig.10

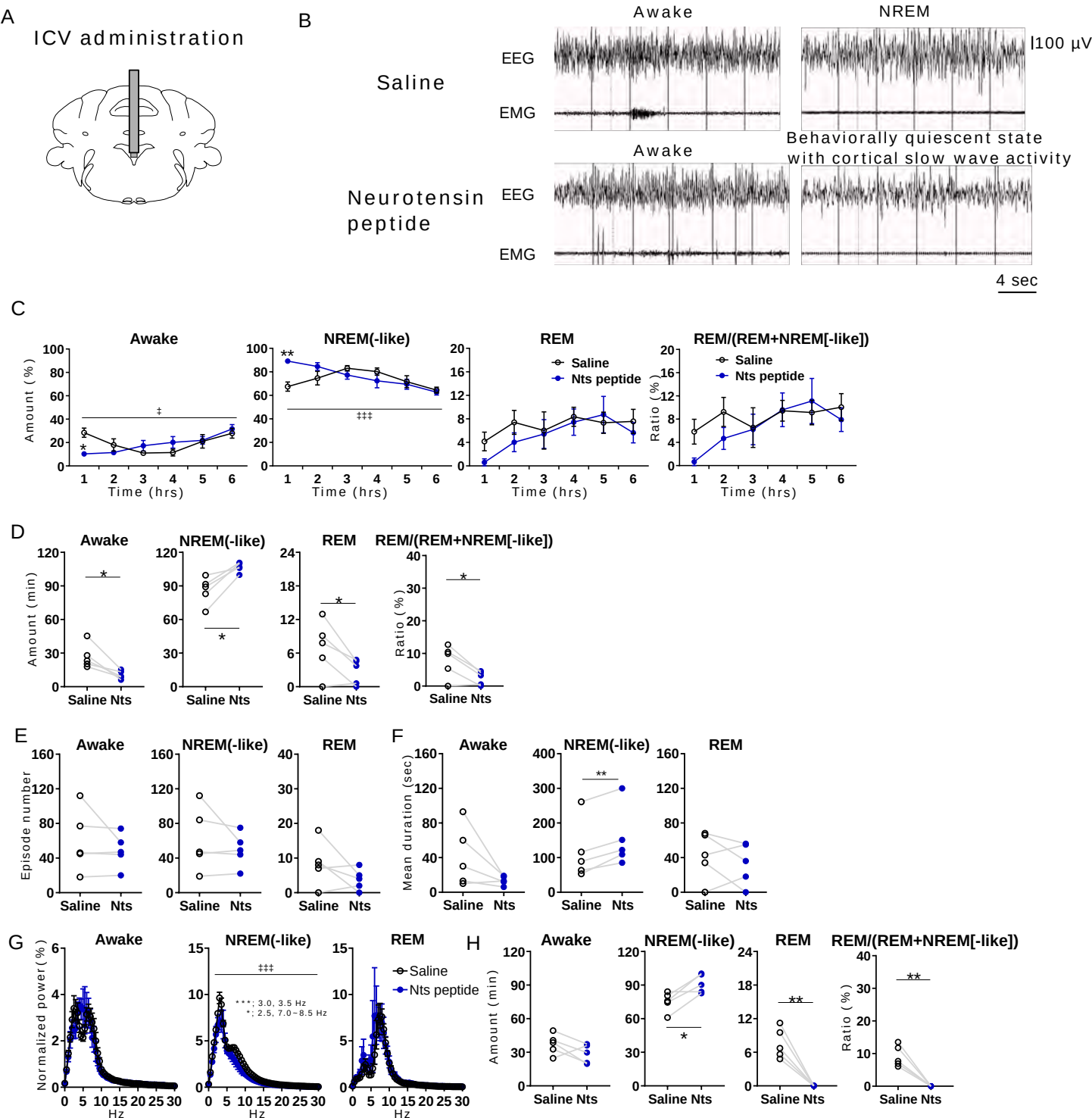
A
ICV administration
B
Awake
NREM
Saline
EEG
EMG
100 μV
Behaviorally quiescent state
with cortical slow wave activity
Neurotensin peptide
4 sec
C
Awake
NREM(-like)
REM
REM/(REM+NREM[-like])
Saline
Nts peptide
Amount (%)
Ratio (%)
Time (hrs)
D
Amount (min)
Saline Nts
E
Episode number
F
Mean duration (sec)
G
Normalized power (%)
***: 3.0, 3.5 Hz
*: 2.5, 7.0-8.5 Hz
Hz
H

Fig.11

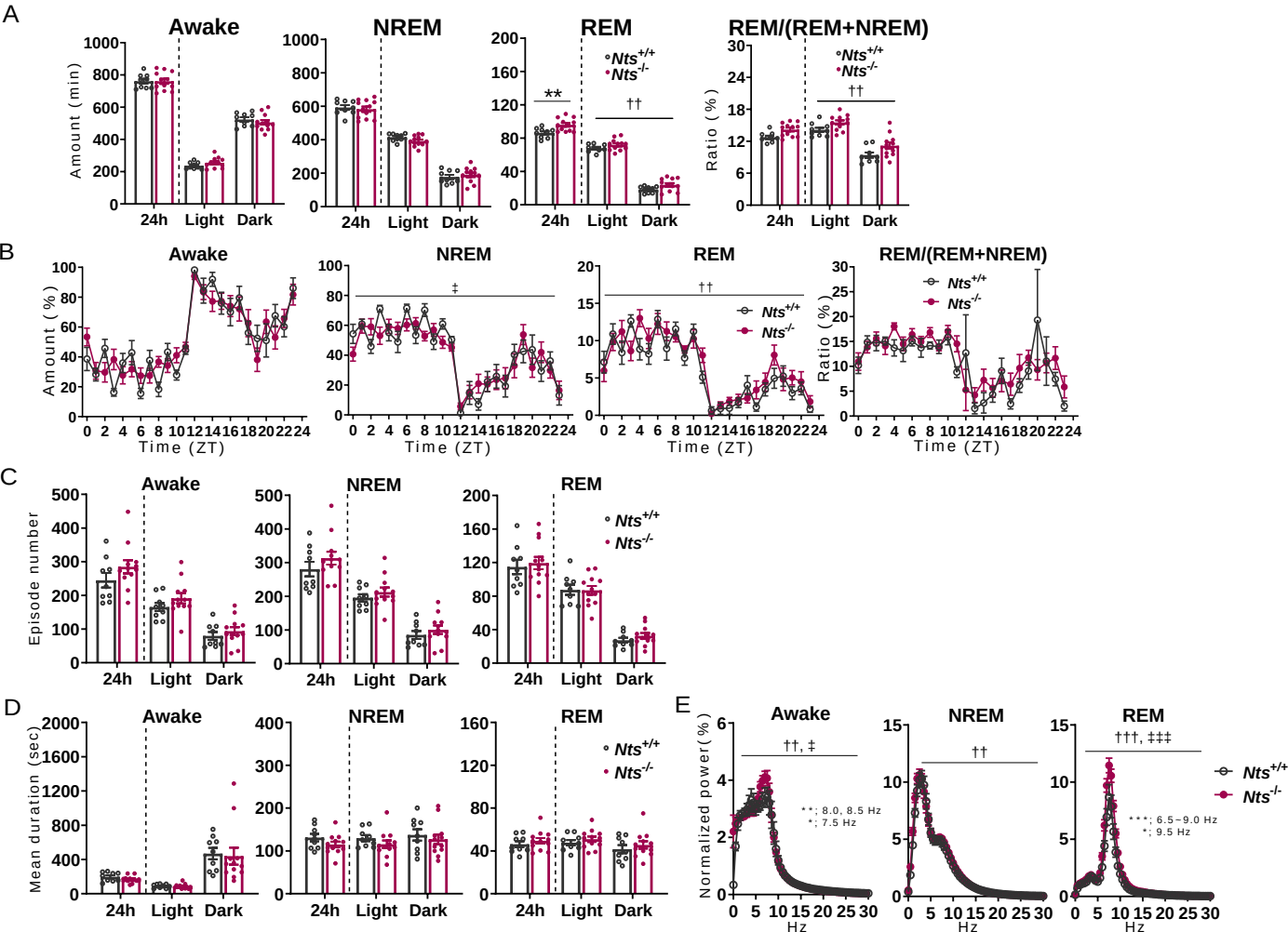
A
Awake
NREM
REM
REM/(REM+NREM)
Amount (min)
Ratio (%)
Nts+/+
Nts-/-
**
††
24h
Light
Dark
B
Amount (%)
‡
Time (ZT)
C
Episode number
D
Mean duration (sec)
E
Normalized power(%)
††, ‡
††
†††, ‡‡‡
**; 8.0, 8.5 Hz
*; 7.5 Hz
***; 6.5~9.0 Hz
*; 9.5 Hz
Hz